The Application of Photosynthetic Materials and Architectures to Solar Cells

by

Jonathan King Mapel

B.S. Electrical Engineering, University of Southern California, 2003

Submitted to the Department of Electrical Engineering and Computer Science
in partial fulfillment of the requirements for the degree of

Master of Science in Electrical Engineering and Computer Science

at the

MASSACHUSETTS INSTITUTE OF TECHNOLOGY

January 2006

Author .....
Department of Electrical Engineering and Computer Science
January 20, 2006

Certified by .....
Marc A. Baldo
Esther and Harold Edgerton Assistant Professor of Electrical Engineering and Computer Science
Thesis Supervisor

Accepted by .....
Arthur C. Smith
Chairman, Department Committee on Graduate Theses
Electrical Engineering and Computer Science

The Application of Photosynthetic Materials and Architectures to Solar Cells

by

Jonathan King Mapel

Submitted to the Department of Electrical Engineering and Computer Science
on January 20, 2006, in partial fulfillment of the
requirements for the degree of
Master of Science in Electrical Engineering and Computer Science

Abstract

Photosynthetic approaches to redesigning photovoltaics (PV) offer an attractive route towards achieving high-efficiency, low-cost solar energy transduction. This thesis explores two routes toward this end: the direct integration of photosynthetic structures into solid-state devices and the architectural redesign of organic solar cells to more closely parallel photosynthesis.

The highly efficient photosynthetic reaction center is the site of exciton dissociation in photosynthesis, analogous to the role of the donor-acceptor interface in organic PV. This thesis describes the successful integration of reaction centers with organic semiconductors into solid-state devices. Although functional, we find that these devices suffer the same limitation as the more traditional organic PV: the ability to absorb enough light.

Photosynthetic bacteria and plants compartmentalize the processes leading to light energy conversion. This spatial separation of structures augments the evolutionary design space: the processes of photon absorption and exciton dissociation occur in two separate locations, allowing the independent functional optimization of each. Applying a similar approach to PV would similarly remove the need for multifunctional materials, bypassing limiting tradeoffs and permitting the utilization of new material systems. To this end, I propose a novel architecture and present initial conclusions on theoretical performance efficiency. Fabricated devices demonstrate the system is viable and suggests that further improvements in device design will enable highly efficient photovoltaics.

Thesis Supervisor: Marc A. Baldo
Title: Esther and Harold Edgerton Assistant Professor of Electrical Engineering and Computer Science

Acknowledgments

I am indebted to my research supervisor, Marc Baldo for his direction and guidance in this work.

I acknowledge the numerous persons whose efforts were involved in the results presented here. These include: Tim Heidel, Kemal Celebi, Rupa Das, Patrick Kiley, Michael Segal, and Madhusudan Singh.

I thank my partner, Audrey Lee, for her love and support.

My research was undertaken with the support of a National Defense Science and Engineering Graduate Fellowship.

The contents of this thesis closely parallel the chapter entitled "The Application of Photosynthetic Materials and Architectures to Solar Cells," to be published in Nanostructured Materials for Solar Energy Conversion, (ed. Soga, T.) (Elsevier, Amsterdam, 2006).

Contents

List of Figures

Chapter 1

Why Photosynthesis?

Widespread adoption of solar cells remains limited by their high cost per Watt of generated power.[1] This is due in part to the expensive equipment and energy hungry processes required in the manufacture of conventional semiconductor-based photovoltaic (PV) cells. On the other hand, PV cells made from organic semiconductors such as films of molecules or polymers hold the promise of low cost production. For example, one class of suitable molecular PV materials, the phthalocyanine pigments,[2] are currently produced in quantities exceeding 80,000 t annually.[3] In addition, this inexpensive feedstock is compatible with high throughput web processing. The printing, paint, and packaging industries routinely spray-coat, stamp, and evaporate molecular and polymeric materials onto flexible plastics and foils.[1] If similar web-based processing is realized for organic PV cells, organic devices need only reach performance levels commensurate to inorganic PV technologies to decrease the cost per Watt of PV power.

Organic PV power efficiencies have steadily improved, reaching approximately 5% in recent results [4, 5] still substantially below that of more mature conventional technologies.[6] But conventional semiconductor solar cells are not necessarily the most appropriate model for the development of organic PV. The physics of organic PV cells is much closer to that other, much older and more sophisticated, example of organic electronics: photosynthesis.

Photosynthesis efficiently converts solar to electrical energy, which then drives a

series of chemical reactions. This ubiquitous, time-tested energy transduction method is the source of all current biomass and, over geologic timescales, all the fossil fuels relied upon today and sustains life on Earth.[7] Photosynthetic plants and bacteria utilize organic molecules similar to those used in organic PV to fix more than 100 Gt of carbon annually, equivalent to 100 TW, a feat accomplished without high temperature processing or huge initial energetic expenditures. From a manufacturing standpoint, the utilization of photosynthetic organism represents the ultimate in low cost processing. A field of switchgrass, for example, can be grown at very low cost but produces the raw material equivalent to several times its area in PV cells *annually* (see section 2.2.4).

In Part II of this chapter, I will compare organic PV to photosynthesis. The principal challenge in organic PV is to absorb sufficient light in the vicinity of charge generation interfaces. I discuss the different architectures employed in photosynthesis and organic PV to address this problem. The direct integration of photosynthetic protein structures into photoelectric devices constitutes one route towards achieving efficient and low cost organic PV. In Part III, I summarize work in hybrid solid state photosynthetic devices. In Part IV, I discuss the implementation of photosynthetic architectures with separate light absorption and charge generation structures in synthetic organic PV cells. Finally, I discuss the prospects for photosynthetic materials and architectures in organic PV.

Chapter 2

Organic PV and Photosynthesis Compared

2.1 Organic PV

I begin by briefly reviewing the processes and structures commonly used in organic semiconductor heterostructure PV. For an in depth review of these devices, see Peumans, 2003.[8] Similar to their inorganic counterparts, organic PV devices are comprised of donor and acceptor semiconducting regions sandwiched between conducting electrodes. Usually, these materials are different semiconductors, as reliable doping to control majority carrier type is difficult to achieve.

The sequence of processes yielding light to electrical energy transduction in organic PV can be divided into four phases, as summarized in figure 2-1. In the first, upon optical excitation in one or both organic materials, localized Frenkel or charge transfer excitons are generated.[9, 10] These tightly-bound, charge-neutral species diffuse until they recombine or dissociate. Excitons that reach an interface between the donor and acceptor layers will dissociate if the energetic offsets favor the process. For large offsets, dissociation occurs over time scales of a few hundred femtoseconds [11] and results in free electrons in the lowest unoccupied molecular orbital of the electron transport material and free holes in the highest occupied molecular orbital of the hole transport material. These free carriers diffuse out towards the contact and are

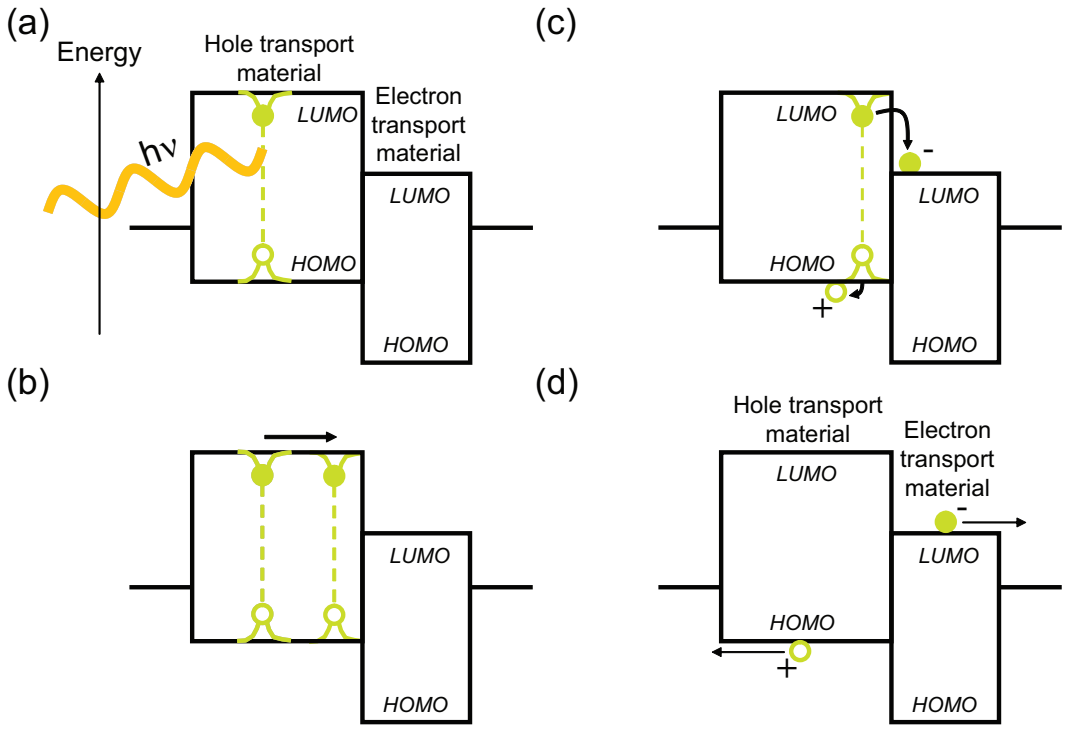

Figure 2-1: **Summary of processes in organic PV resulting in photocurrent generation** (a) Optical absorption in one or more active semiconducting layers creates an exciton, an electron-hole pair localized on a single molecule. (b) Excitons diffuse in the thickness of the film. (c) Those that reach the interface between the donor and acceptor layers can dissociate. In this example, an excited molecule in the donor hole transport material reduces an nearby acceptor molecule in the adjacent electron transport material. (d) The separated free electrons and holes diffuse out towards the metal electrodes, completing the energy transduction process.

available to perform electrical work.

The useful thickness of an organic PV cell is restricted to the distance that excitons can travel before recombining, typically on the order of 10 nm.[8] Within this region the internal quantum efficiency (the ratio of charge extracted to absorbed photons) can be 100%. But the quantum efficiency drops dramatically in thicker devices due to exciton recombination losses.[12] Thus, despite optical absorption coefficients exceeding $10^{-5}\,\mathrm{cm}^{-1}$ averaged over the visible spectrum, organic PV is limited by an inability to absorb enough light. Several classes of solar cells have emerged whose device architectures address this concern, including dye-sensitized nanostructured oxide cells, [13] bulk organic heterojunction cells, [5, 14] and organic-inorganic hybrid

composites.[15, 16, 17] These approaches share the characteristic of increased surface area of the exciton dissociation interface, increasing the useful thickness of the cell.

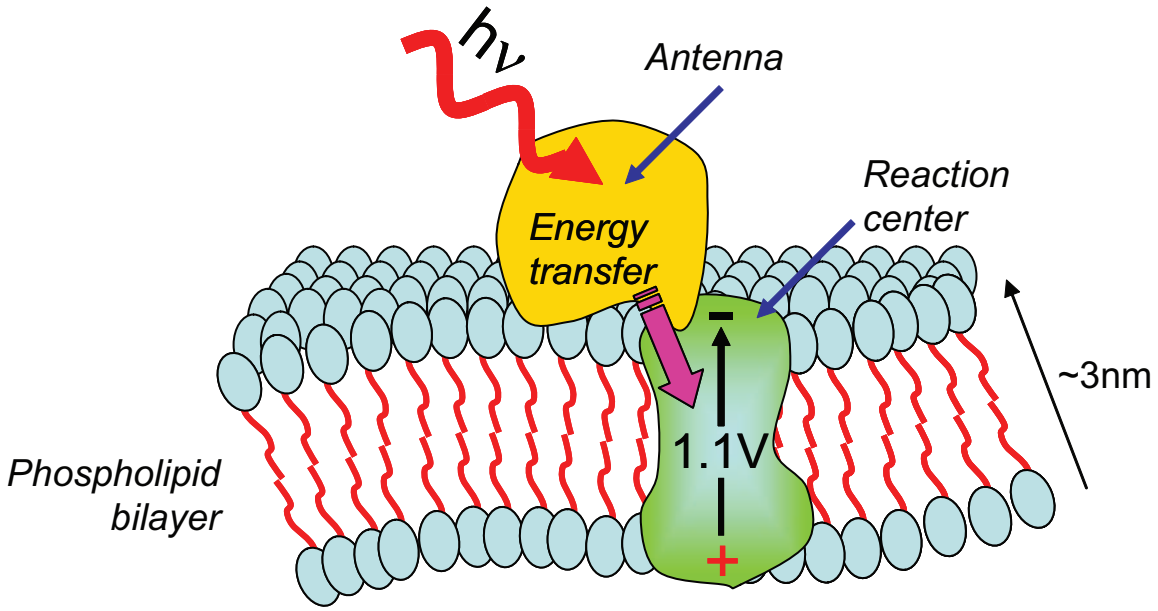

Figure 2-2: **Schematic diagram of photosynthetic membrane**, showing the spatial distribution of the light harvesting antenna and reaction center, the sites of photon absorption and exciton dissociation, respectively. In photosynthesis the energy transduction machinery are protein complexes that house optically active molecular components embedded in a phospholipid membrane. After Purves, et al.[18]

2.2 Photosynthesis

Photosynthesis also maximizes its active surface area by embedding charge generation components into a flexible membrane. But in contrast to organic PV, the architecture of photosynthesis employs separate components for light absorption and charge generation, allowing these two functions to be optimized independently. Overall, photosynthesis can be divided into three distinct phases: (1) light absorption and energy transport by antenna systems, (2) energy collection and charge separation in reaction centers, and (3) stabilization by secondary reactions for use in the synthesis of sugars. The first two components are the biological equivalent of a PV cell, albeit with a very

different architecture; see figure 2-2.

2.2.1 Photosynthetic Antenna Complexes

All photosynthetic organisms contain light-gathering antenna systems, as such, they are remarkably diverse. Antenna types can be divided into several categories: (1) light harvesting complexes of purple bacteria, (2) light harvesting complexes of plants and algae, (3) phycobilisomes of cyanobacteria and red algae, (4) peridinin-chlorophyll proteins of dinoflagellate algae, and (5) chlorosomes of green bacteria. We refrain from an extensive discussion of all antenna types, as excellent reviews can be found elsewhere.[19]

Antennas contain high concentrations of pigment molecules, including chlorophylls, bilins, carotenoids, and their derivatives. Photons captured by these pigments generate excitons, as in organic PV. But unlike the semiconducting films in organic PV which rely on diffusion, many antenna complexes are designed to guide excitons to reaction centers. For example, phycobilisomes possess pigments at the periphery of the complex that absorb at higher energies than those at the core. Excitons at the periphery travel via Förster energy toward the core where they are coupled to the reaction center.

Most antenna systems are comprised of pigment-protein complexes where the photoactive pigment cofactors are positioned by a protein matrix, altering their optical properties and controlling energy transfer. Chlorosomes are an exception: as perhaps the only example of solid-state semiconductors in nature, they are of particular interest to organic PV. They are unique in that they are largely composed of pigments ($> 50\%$ by dry weight [19]) and constitute the most efficient light harvesting complexes found in nature.[20] The green photosynthetic bacteria that possess chlorosomes are frequently found in volcanic hot springs where the ambient temperature reaches 47°C.[21] Such extreme conditions may have contributed to the unique structure of chlorosomes, but they also appear especially well adapted to conditions of extremely low light flux. Compared to other photosynthetic antennas, they have very high absorption cross sections.

While several models have been proposed for the pigment organization in chlorosomes, a common characteristic is the existence of aggregates of bacteriochlorophyll c, either rods of 5-10 nm in diameter and 100-200 nm in length [22, 23, 24, 25, 26] or semicrystalline lamellar sheets.[20] The regular structure of Bchl c van der Waals bonded aggregates leads to strong exciton coupling and a red-shift in absorption. Crystallinity over 100 nm length scales and exciton delocalization make the Bchl c aggregates highly desirable for use as organic semiconductors in organic PV; materials with these characteristics are currently under development for use in organic electronic devices.[27, 28, 29, 30]

2.2.2 Photosynthetic Reaction Centers

In photosynthesis, the role of the donor-acceptor interface is performed by the reaction center. The dissociation of excitonic energy states and formation of separated charges occurs at the reaction center via a series of electron transfer reactions. The reaction center is a membrane-bound, multisubunit, pigment-protein complex which incorporates chlorophyll derivatives and other electron transfer cofactors such as quinones. The pigments and cofactors are held together by van der Waals interactions with the protein matrix; their positioning and orientations are important in facilitating electron transfer.

The ultimate collection point for excitons from neighboring antenna complexes is a chlorophyll dimer in the reaction center known as the special pair. This is the lowest energy site in the photosynthetic optical circuit. It is also the primary electron donor for the subsequent electron transfer cascade that carries the electron across the membrane while the hole remains at the special pair, thereby separating the exciton into isolated charges; see figure 2-3. Recombination, or the back transfer of the electron to the special pair, is prevented by the electron transfer cascade which occurs in a series of very fast (1-100 ps) electron transfer reactions, rapidly separating the charges to $\sim 3\,\mathrm{nm}$ and strongly decreasing the rate of recombination. Exciton dissociation in reaction centers thus proceeds with high efficiency; the quantum yield of products to photons is nearly unity.[31] The potential of the separated charges

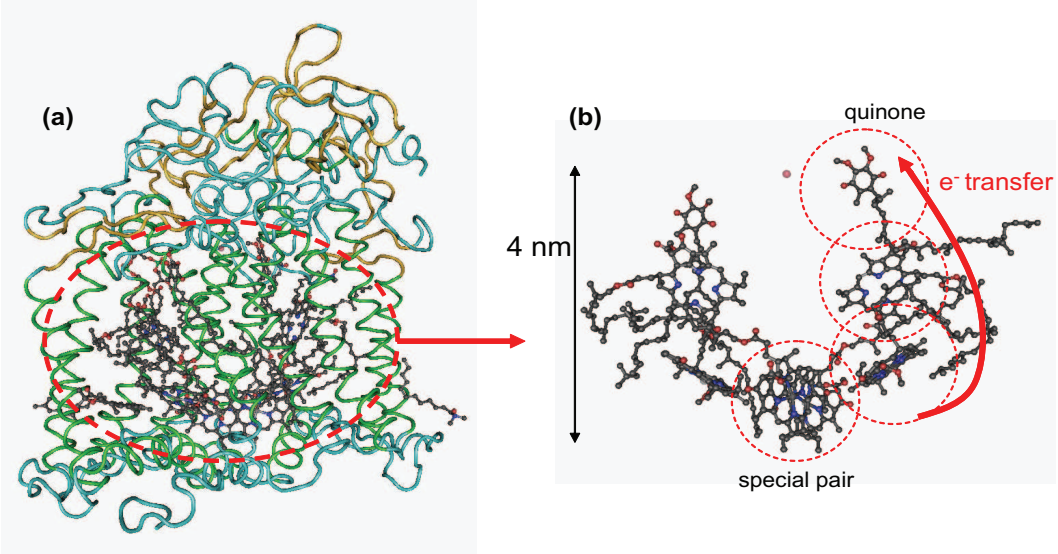

Figure 2-3: **Structure of the reaction center complex of *Rhodobacter spaeroides*** (a) Entire complex, including the L, M, and H subunits and cofactors. (b) Cofactors only. The special pair is the primary electron donor of the electron transfer cascade, illustrated by the arrow. Figure produced from the Protein Data Bank file 1AIJ using Visual Molecular Dynamics.[33]

varies from approximately 0.5 V in primitive purple bacteria, to approximately 1.1 V in more advanced systems [32]. The secondary reactions that follow stabilize the oxidized and reduced species, yielding a chemical potential across the photosynthetic membrane that can then be used to drive cellular metabolism. The rapid, multi-step spatial separation achieved in reaction centers may reduce their recombination losses relative to less sophisticated donor-acceptor interfaces in organic PV.

Unlike antenna complexes, reaction center complexes are remarkably well preserved across plants and photosynthetic bacteria. All reaction centers follow the above described general structure of electron transfer cofactors embedded in a protein matrix. In plants and cyanobacteria, two special reaction centers called photosystems I and II operate in tandem to split water and create molecular oxygen, a highly energetic reaction since water is an extremely poor electron donor. Oxygen produced by photosynthesis is the source of oxygen in the atmosphere and fundamentally affected the development of life on Earth.

2.2.3 Efficiency of Photosynthesis

The efficiency of energy transduction of photosynthesis varies depending on which subset of the complete cycle is considered. The quantum efficiency (photon to separated charge) at low to moderate intensities is nearly 100%, as nearly every photon absorbed drives photochemistry. If the efficiency is defined as the fraction of energy absorbed by the organism operating under ideal conditions that is converted to carbohydrates and oxygen, the efficiency of energy storage is 27%.[31] Under more practical lighting and conditions, this efficiency decreases to 5%.[34] When cellular metabolic processes are included, the proportion of energy converted to biomass is about 0.2%.[35]

In solar photovoltaics, extracted energy is stored in the form of separated charges that possess a difference in chemical potential energy. When there are no free charges, as in a chemical solar cell, extracted energy exists in the form of binding energy of the molecular products of the cell.[36] The processes of photosynthesis are a form of chemical solar cell and as such, the photosynthetic equivalent is energy stored in the chemical bonds of carbohydrates and oxygen.

At 5%, the efficiency of photosynthetic energy conversion and state of the art organic PV are similar, despite their dramatic structural differences. However, since the products of an electrical solar cell are more useful in the modern economy than those of a chemical solar cell, additional energy transduction steps would need to be included to make a direct comparison; the most direct conversion mechanism entails the operation of an electrochemical cell.

2.2.4 Agricultural Production of Solar Cell Raw Materials

The attractiveness in using agriculture as a low cost manufacturing method has motivated researchers in the fields of energy and medicine for decades. Agricultural production for solar cells is similarly impelling. An estimate for the amount of raw materials which could be used to produce PV is heavily dependent on the method of estimation and the attendant assumptions. I estimate here that a field of crops would

provide the raw materials for five times its area in PV.

The details of this calculation are as follows. Photovoltaics made from organic semiconductors commonly consist of thin, amorphous films of semiconductors. I assume that photosynthetic pigment molecules, mainly chlorophyll, would take on this role in photosynthetic PV in an identical role. The total number of chlorophyll molecules can be calculated by assuming a molecular density in the thin film and a film thickness. The molecular density of bacteriochlorophyll *c* in the chlorosomes of green photosynthetic bacteria is $2 \times 10^{21}\,\mathrm{cm}^{-3}$.[37] This is nearly identical to the molecular density of copper phthalocyanine molecules in thin films, justifying the validity of this assumption.[38] Assuming an active film thickness of 1 µm, $\sim 2 \times 10^{17}$ chlorophyll molecules are needed per square cm of PV cells.

To determine chlorophyll production rates, switchgrass (*Panacum virgatum* L.) was chosen as the model organism. Switchgrass grows quickly as is currently being investigated as a biofuel energy crop for cofiring fuel in coal plants.[39] The dry matter yield of switchgrass is assumed to be 15×10^6 g per hectare per year.[39] I then assume that 80% of this weight originates from grass leaves. The specific leaf weight (dry matter weight per surface area of exposed leaf) of switchgrass is roughly 40 $\mathrm{g/m}^2$.[40] As an estimate for the number of chlorophyll molecules per unit of exposed leaf surface area, I use 3×10^{16} per cm^2.[41]

Assuming a field encompasses roughly 8 hectares, these growth rates result in $3 \times 10^5\,\mathrm{m}^2$ of PV raw material per field annually. Stated as the ratio of land necessary for production, agricultural methods could produce enough raw material to make five times its area annually in solar cells. However, as with more mature silicon technologies, the cost of raw material may not be the main determinant of end energy cost.

Chapter 3

Integration of Photosynthetic Complexes in Organic Photovoltaics

Much of the initial work on organic PV utilized thin films of molecules structurally similar to the chlorophyll pigments of photosynthesis.[42] Such devices, however, have not approached the efficiency of photosynthesis. Equating the potential developed across a photosynthetic reaction center to the open circuit voltage of a solid-state solar cell yields a photosynthetic power conversion efficiency exceeding 20% and potentially competitive with the best silicon devices. This high performance is a consequence of the unique molecular scale engineering of photosynthetic complexes. Thus, the prospect of using photosynthetic complexes directly is tempting, as agriculture constitutes a far less expensive manufacturing route compared to semiconductor foundries.

3.1 Self Assembly of Photosynthetic Complexes

The first step in the construction of a device containing photosynthetic complexes is the assembly of the biological structures on a substrate. The self-assembled structure may then be employed as an electrode in an electrochemical cell, or integrated in a solid-state PV cell. The goals for this self-assembly are: (1) to uniformly orient complexes to minimize recombination losses, and (2) form an optically dense film to

increase absorption.

Self-assembly technology for photosynthetic complexes was pioneered in wet electrochemical cells.[43] This section is not intended as a comprehensive description of the history of photosynthetic materials in electrochemical cells, but the work of Katz on the self assembly of bacterial reaction centers (RCs) is especially notable [43]. Using cysteine binding to reaction center complexes Katz demonstrated wet electrochemical cells with internal quantum efficiencies as high as 60%. Following the work of Katz, Lebedev et al. [44] investigated the self-assembly of oriented films of photosynthetic complexes on transparent and conductive indium-tin oxide (ITO) surfaces using $Ni^{2+} - NTA$ binding to His_6 tags on genetically engineered RCs from the *Rhodobacter sphaeroides* strain SMpHis, [45] shown schematically in figure 3-1. Lebedev et al. found that binding to His_6 tags increased the photocurrent despite a theoretical increase in the length of the linker molecule connecting the RC to the substrate.[46] A typical tapping mode atomic force microscopy (TM-AFM) image of a His_6-RC self-assembled monolayer on atomically flat Au-on-mica substrates is shown in figure 3-1c. Although there is significant disorder in the film, it is relatively closely packed.

The self-assembly technology of photosystem 1 (PSI) is less developed. Greenbaum et al. have demonstrated preferential orientation of PSI by engineering the surface chemistry of gold.[47] By controlling the surface charge and hydrophobicity, they demonstrated several possible orientations of PSI on modified gold. An alternative technique allows a single His_6 tag to be introduced to native PSI complexes in a three-step process; see figure 3-2a. Minai et al. [48] have demonstrated that the native psaD subunit of PSI may be exchanged and replaced by a genetically engineered psaD with His_6 tagged onto the C-terminus.

To investigate the orientation of PSI bound by psaD exchange we performed TM-AFM phase imaging [49] in the intermittent contact mode and varied the potential between the AFM tip and the ITO/Au substrate.[50] The phase angle of the driven vibration of the cantilever in TM-AFM is related to the energy dissipated in the tip-sample interaction.[49] Thus, phase images of biological materials provide a map

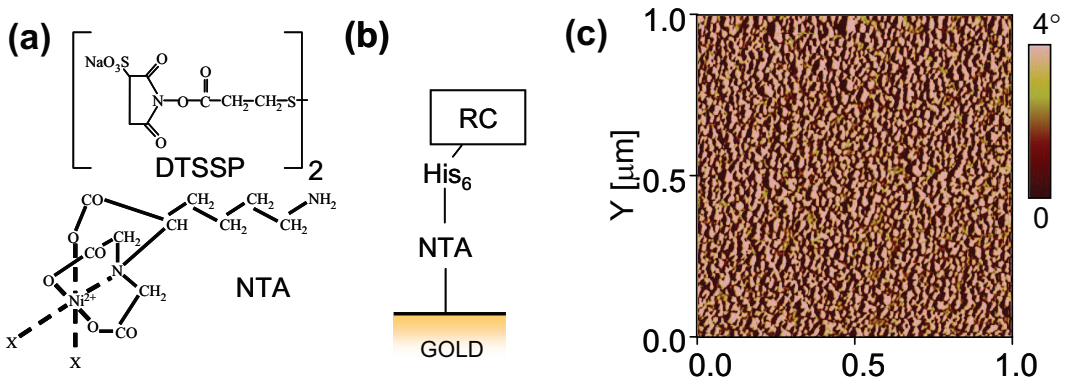

Figure 3-1: **Method for oriented assembly of reaction centers on Au** (a) The substrate is treated with 3,3ť-Dithiobis[sulfosuccinimidylpropionate] (DTSSP) and nickel 2+ nitrilotriacetic acid (Ni-NTA). (b) A polyhistidine (6) tag on the reaction center expressed from *R. sphaeroides* chelates the charged Ni ion of the Ni-NTA, immobilizing and orienting the complex on the substrate. (c) Atomic force microscopy image of assembled reaction centers on gold.

of the dissipative part of their mechanical response. When a potential is applied to the AFM tip, we can alter its mechanical interactions with polar or charged samples by, for example, aligning polar molecules in the electric field.[51] Voltage-dependent phase scans of a likely PSI particle is shown in figure 3-2b-d. Phase scans taken at +1 V and 0 V show little difference, but phase scans taken at -1 V exhibit the appearance of localized regions of increased phase. The increase in phase in the -1 V scan corresponds to an increase in the attractive forces between the tip and the sample [49] and indicates the presence of a positive charge trapped on the surface of PSI, mostly likely at P700. Thus, the voltage dependence of TM-AFM phase imaging is consistent with the expected rectifying characteristics [47] of PSI in the orientation prescribed by the self-assembly technique of figure 3-2a. The packing density of PSI is, however, far less than optimal, most likely due to incomplete exchange of psaD.

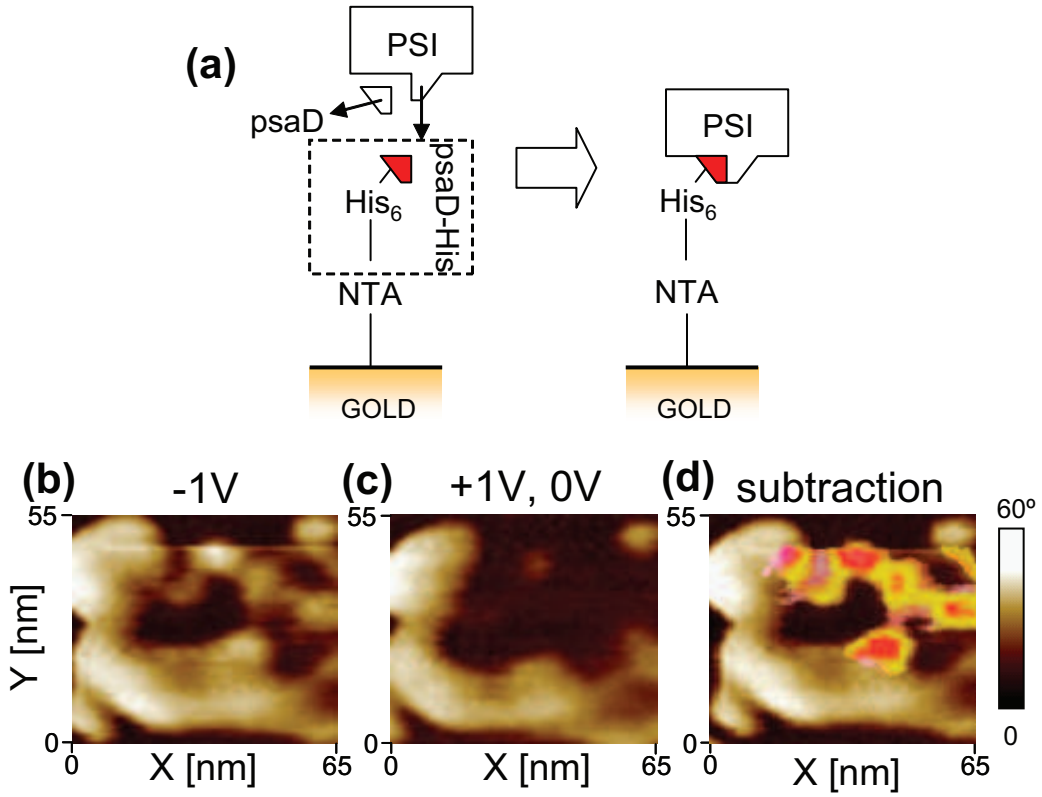

Figure 3-2: **Method for oriented assembly of PSI onto Au** (a). As with reaction centers, the substrate is treated with DTSSP and Ni-NTA. A polyhistidine tag is introduced to PSI by assembly of an engineered psaD subunit then exposing the surface to native PSI such that the subunit is substituted.[48] TM-AFM phase images of assembled PSI on Au at (b) -1 V, (c) 0 V, and +1 V. The image difference (d) shows localized regions of increased phase, signifying a change in dissipative energy corresponding to tip interactions with a positively charged PSI complexes.

3.2 The Stability of Photosynthetic Complexes in Solid State

The rinsing and drying steps required during fabrication of solid-state photosynthetic devices are particularly prone to damage the photosynthetic complexes. The integrity of these large complexes can be increased with the use of surfactant stabilizers.[52] To quantify the effect of stabilization, the low temperature fluorescent spectrum is measured. After excitation by a pump laser at $\lambda = 408\,\mathrm{nm}$ with intensity $0.5\,\mathrm{mW/cm^2}$, protein degradation is recognized by wavelength shifts in fluorescence. The chloro-

phyll molecules associated with the PSI complex provide an intrinsic steady-state fluorescence spectrum at $T = 20\,\mathrm{K}$ between $650 < \lambda < 800\,\mathrm{nm}$ that reflects the organization of the pigment-protein interactions. Thick, vacuum-dried films of PSI prepared directly on glass substrates prior to functionalization exhibit a large blue shift of the fluorescence maxima from $\lambda = 735\,\mathrm{nm}$ to $\lambda = 685\,\mathrm{nm}$, indicating a disruption in light harvesting subunit organization. Polyelectrolytes such as polyethylene glycol, that have been used to preserve dried biological materials,[53] were not found to improve the stability of PSI. In contrast, incubating PSI with the peptide surfactants A_6K/V_6D [54, 55, 56, 57] was found to almost entirely preserve its low temperature fluorescent spectrum;[52] see figure 3-3. The $\lambda = 735\,\mathrm{nm}$ fluorescent peak of peptide-stabilized films stored in an ambient environment exhibited a gradual blue shift over several weeks, indicative of gradual structural changes in the light harvesting antennae of PSI.[58] The low-temperature fluorescent data demonstrates that PSI can be successfully integrated in a solid-state environment.

3.3 Solid State Integration of Bacterial Reaction Centers

To date, wet electrochemical implementations of photosynthetic PV cells have not succeeded in realizing efficient devices. In many photovoltaic applications, wet cells require additional packaging and are hampered by stability concerns.[59] Furthermore, diffusion-limited charge transport in the electrolyte increases the series resistance, lowering the fill factor. Consequently, it is desirable to demonstrate technology for integrating biological protein-molecular complexes with solid-state electronics.

The simplest model of a solid-state photosynthetic device consists of uniformly oriented photosynthetic protein-molecular complexes deposited between two metallic contacts. After absorption of a photon and rapid charge separation within a complex, a potential of up to 1.1 V can be developed across the metal contacts.[32, 60] However, this model of a solid-state photosynthetic device must overcome several practical

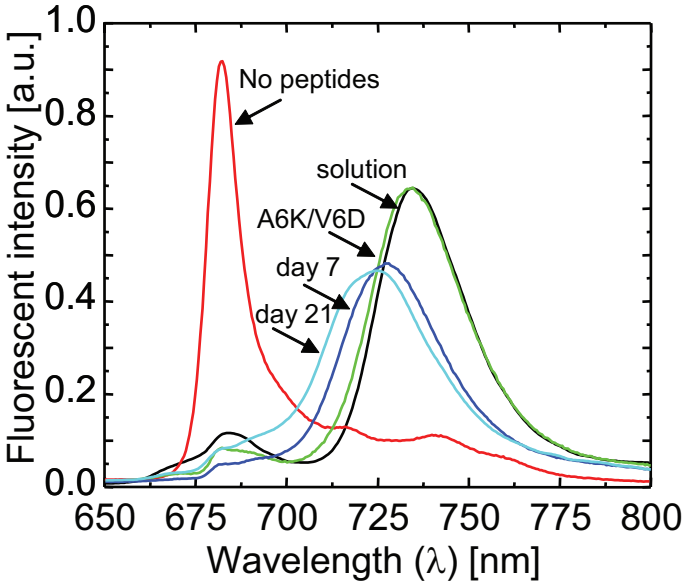

Figure 3-3: **Fluorescence measurements of assembled PSI on Au** Comparison between the low temperature (T = 10 K) fluorescence spectrum of PSI solution as extracted from spinach, with washed and dried films of PSI, demonstrates that PSI may be protected against degradation after washing and drying steps by stabilizing the complex with surfactant peptides A_6K and V_6D. The excitation source was a pump laser at $\lambda = 408\,\mathrm{nm}$ with intensity $0.5\,\mathrm{mW/cm^2}$. The 50 nm blue shift of assembled PSI without peptide surfactants shows the disruption of PSI light harvesting unit organization. The stabilizing action of A_6K/V_6D is preserved for several weeks for dried films left in ambient conditions.

obstacles. First, the optical cross section of a single layer of photosynthetic complexes is fairly low; second, deposition of the top metallic contact may cause damage to biological materials; and finally, defects in the layer of photosynthetic complexes may permit electrical shorts between the metallic contacts. The two latter problems are circumvented by depositing a thin ($< 100\,\mathrm{nm}$) layer of an amorphous organic semiconductor between the photosynthetic complexes and the top metal contact. The semiconductor transports the photogenerated electrons to the cathode of the cell.

The energy level structure of an RC-based photovoltaic cell is shown in figure 3-4a. RCs are oriented using a His_6 tag with the electron-accepting special pair facing the substrate. Fabrication of solid state cells begins with self-assembly of the A_6K/V_6D stabilized photosynthetic complexes as in electrochemical cells. But after the complexes are self-assembled on a functionalized electrode, they must be washed

with deionized water to remove unbound material and excess salt and detergent from the buffer. Since solid-state devices are much thinner than electrochemical cells, they are less tolerant of debris on the substrate. The RC-based photovoltaic cell employs a 60 nm-thick protective layer of the fullerene C_{60}. C_{60} was chosen because of its relatively deep lowest unoccupied molecular orbital (LUMO) energy of 4.7 eV [61] that should enhance electron transfer from the electron acceptor in the RC. It is observed that C_{60} transports electrons in its LUMO far more readily than holes in its highest unoccupied molecular orbital (HOMO). Consequently, C_{60} is employed as an electron transport layer (ETL). After C_{60}, a 12 nm-thick layer of a second ETL 2,9-dimethyl-4,7-diphenyl-1,10-phenanthroline (bathocuproine, or BCP)[62] is deposited and finally, an 80 nm-thick layer of Ag is deposited through a 1 mm-diameter shadow mask. Thermally-evaporated films of C_{60}, BCP, and Ag were deposited at a rate of $\sim 0.3\,\mathrm{nm/s}$ in a vacuum of $< 10^{-6}\,\mathrm{Torr}$. The Ag deposition likely damages the thin BCP layer, facilitating electron extraction.[63] But even in a damaged layer, the deep HOMO of BCP effectively prevents the injection of holes into the device, markedly improving the device's reverse bias characteristics [50].

The current-voltage characteristics of the RC-based photovoltaic cell are shown in figure 3-4b. Under illumination at $\lambda = 808\,\mathrm{nm}$, where C_{60} and BCP are transparent,[8] the device exhibits photocurrent in reverse bias, i.e. the ITO is negative relative to the top Ag contact. Most notably, the device exhibits photovoltaic behavior, albeit weak, with an open circuit voltage that varies slightly between devices but is typically 0.10 V and a short circuit current density of $0.12\,\mathrm{mA/cm^2}$ under an excitation intensity of $0.6\,\mathrm{W/cm^2}$ at $\lambda = 808\,\mathrm{nm}$. Assuming a perfectly formed RC monolayer of density $8 \times 10^{-12}\,\mathrm{mol/cm^2}$, and given an extinction coefficient of $2.9 \times 10^5 M^{-1}\,\mathrm{cm^{-1}}$, [64] we calculate the optimum photocurrent as $2\,\mathrm{mA/cm^2}$, where we have ignored possible interference effects due to reflections from the ITO/Au electrode, and assumed 100% reflection of the optical pump by the Ag cathode. Thus, at a bias of -1 V, a conservative estimate of the internal quantum efficiency of the device is 6%. The solid-state quantum efficiency of 0.03% at an excitation intensity of $0.6\,\mathrm{W/cm^2}$ at $\lambda = 808\,\mathrm{nm}$ is similar to an photoelectrochemical cell with an external

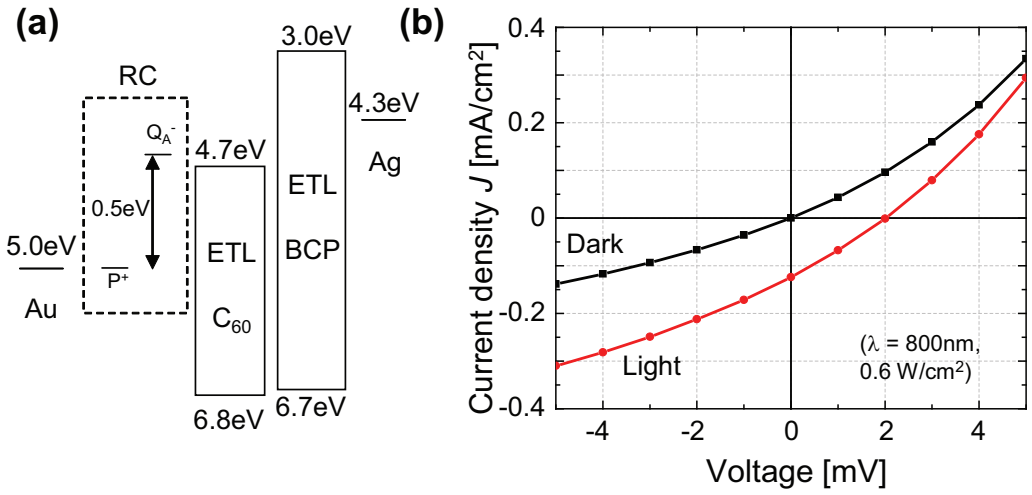

Figure 3-4: **Energy level diagram and current voltage characteristics of an RC solar cell** (a) Device energy levels for the reaction center solar cell. After photoexcitation, electrons localized on the QA anion reduce nearby C_{60} molecules and electrons conduct out the cathode. The energy levels of C_{60} and BCP are from references [61, 62]. (b) The current-voltage characteristics show that under $0.6\,\mathrm{W/cm^2}$ illumination, the device has an open circuit voltage of 2 mV and short circuit current density of $1.2\ \mathrm{mA/cm^2}$. The fill factor is approximately 25%.

quantum efficiency of 0.016% under an excitation intensity of $6\,\mathrm{mW/cm^2}$ at $\lambda = 800\,\mathrm{nm}$.[44]

In figure 3-5, verification of the activity of RCs is confirmed by spectrally resolving the short circuit current using a Ti-Sapphire CW laser tunable between $\lambda = 790\,\mathrm{nm}$ and $\lambda = 890\,\mathrm{nm}$. The photocurrent spectrum is compared with both the solution absorption spectrum of the RC complexes, and a photocurrent spectrum of identical RC complexes in a photoelectrochemical cell reproduced from reference [44]. With the exception of a region near $\lambda = 860\,\mathrm{nm}$ the spectra overlap closely.

These RC solar cell devices suffer from both low internal quantum efficiency and low absorption. The latter is more detrimental, as a monolayer of photoactive element make absorption difficult. This limitation is identical to that restricting high performance in organic semiconductor PV devices.

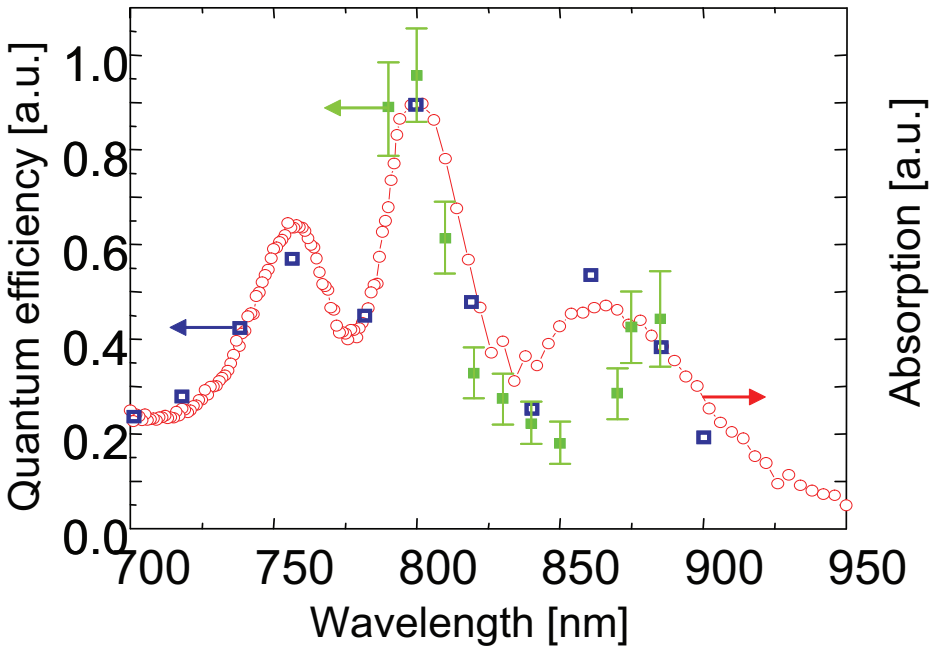

Figure 3-5: **Quantum efficiency spectrum of RC solar cell** The external quantum efficiency (■) calculated from the short circuit photocurrent qualitatively matches both the absorption spectrum of RCs in solution (○) and electrochemical RC photoelectrochemical cell (□) from reference [44].

Chapter 4

Synthetic Implementations of Photosynthetic Architectures

As noted in Part II, the organizational architecture of the initial phases of photosynthesis is different from that of organic PV in at least one major respect. In photosynthesis, light absorption and exciton dissociation occur in the spatially separated components of the antenna and reaction center complexes. In contrast, absorption, exciton dissociation and charge extraction all occur in the organic semiconductors that comprise the active donor and acceptor layers in organic PV. This characteristic frustrates materials selection for organic PV, as the organic semiconductors must simultaneously satisfy several constraints: (1) strong broadband optical absorption with an extinction coefficient of at least $10^5\,\mathrm{cm}^{-1}$ across the visible spectrum, (2) efficient long range exciton transport, (3) optimal energy level alignment for rapid exciton dissociation efficiency, and (4) high electron and hole mobilities and continuous charge pathways to the two electrodes to minimize recombination losses.

Akin to photosynthesis, organic PV may benefit from separating the functions of light absorption and exciton dissociation into two spatially distinct structures, allowing individual optimization of each. We demonstrate separation of optical and electrical functions by utilizing guided wave mediated energy transfer across thin metal films. In such a device, energy transduction proceeds by photon absorption in an 'artificial antenna'. Excited molecular dipoles in the antenna either radiate

into waveguide modes or non-radiatively couple to surface plasmon polariton (SPP) modes in the multilayer structure.

A major advantage of coupling into guided modes is that these modes are absorbed even in very thin organic PV cells, optimized for maximum internal quantum efficiency. Guided modes propagate in the plane of the device, parallel to the charge generation interface. The dimensions of the cell in this plane are on the order of 10^{-2} m, rather than $\sim 10^{-7}$ m perpendicular to the interface. The maximum distance of interaction between a reaction center and a guided mode is thus the distance that these modes travel at visible frequencies. For both SPPs and waveguide modes, they can be several orders of magnitude greater than the thickness of the reaction center, increasing the likelihood they will be absorbed; see figure 4-1.

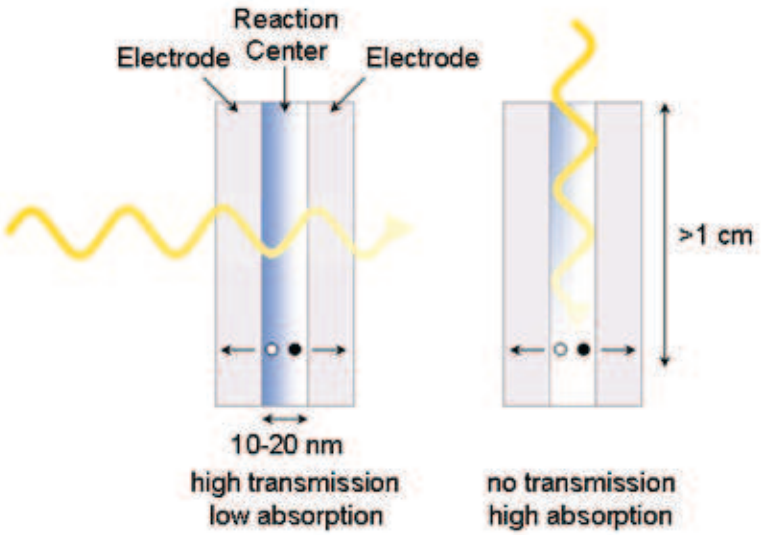

Figure 4-1: **Device excitation routes: perpendicular versus parallel** Excitation of solar cells under normal (perpendicular) (a) and parallel surface mode excitation (b). The interaction distance of the electromagnetic fields and the absorbing artificial reaction center ratio between the two is several orders of magnitude. For very thin PV, high absorption and no transmission is preferred.

Energy which propagates in these guided modes is absorbed in the 'artificial reaction center' of the PV, after which the processes of exciton diffusion, dissociation,

and charge collection occur as before.

4.1 Energy Transfer via Guided Modes

The oscillating electric field of the radiative dipole at an excited molecule in the antenna layer can be damped by several mechanisms, resulting in energy transfer. These mechanisms are: (1) non radiative decay into phonons, (2) radiation of photons into free space modes not guided within the PV, (3) radiation into dielectric waveguide modes in the antenna/PV stack, and (4) non-radiative energy transfer into surface plasmon polariton modes at the adjacent metal interface. Photons in waveguide modes interact with the absorbing active layers in the artificial reaction center identically to normal light illumination.

Non-radiative decay is minimized in efficient antenna dye molecules. Thus, radiation into free space modes is the dominant process for an *isolated* oscillating dipole on an efficient dye molecule. But within a multilayer stack composed of metals and dielectrics, radiation into free space modes is suppressed. This occurs because the rate of photon emission is described by Fermi's golden rule and depends on the photonic mode density. For example, near a metal film, the photonic mode density drops dramatically as visible light is strongly absorbed by the free charges of the metal.

Within a multilayer stack energy transfer to guided electromagnetic modes is preferred. The most important guided modes are surface plasmons polaritons and waveguide modes. The stack acts as a waveguide since its refractive index, $n \sim 2$, higher than air or the glass substrate. Plasmons are quasiparticles comprised of the collective oscillation of the conduction electrons in metals. Surface plasmon polaritons (SPPs) are a unique class associated with interfaces between metals and dielectrics. SPPs propagate along the interface with electromagnetic fields, energy, and charges highly localized within the interface area. Their properties depend strongly on characteristics of both the metal (complex dielectric function, corrugations, roughness) and the dielectric (refractive index). In the absence of the adjacent artificial reaction center, SPPs are internally damped by joule heating in the metal film. Recent ad-

vancements in the ability to control the structure of metals on the nanometer scale have spurred great interest in SPPs in the last decade. Their unique properties are of wide interest in many fields and are being explored for their potential in optics, magneto-optic data storage, microscopy, and sensors.

The existence of SPPs can be straightforwardly derived from Maxwell's equations and the application of appropriate boundary conditions. They are transverse magnetic in character and the existence of surface charge requires an electric field normal to the surface. Since these surface waves propagate along the interface, there is also an electric field in the propagation direction; see figure 4-2. The high density of charges at the interfaces leads to a field enhancement at the interface which decays exponentially with distance from it. This field is referred to as evanescent, reflecting the bound, non-radiative nature of SPPs which restricts power from propagating away from the interface.

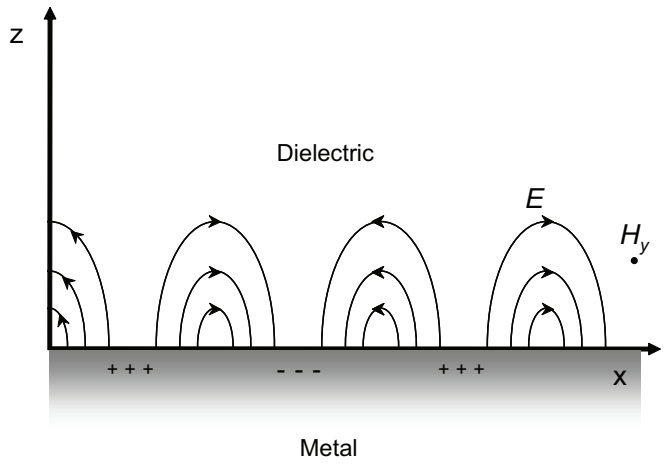

Figure 4-2: **Surface plasmon polariton field orientations** SPPs exhibit magnetic fields that are transverse in character, and the generation of surface charge requires an electric field normal to the surface (after Barnes, et al. [65])

To summarize, there are several advantages to the biomimetic approach of separating light absorption and exciton dissociation in organic PV:

1. By decoupling the optical and electrical components of the solar cell, the ar-

tificial reaction center can be made thinner than the exciton diffusion length, ensuring that all excitons are generated close to the location of exciton dissociation. The efficiency of this process should approach unity, resulting in internal quantum efficiencies approaching unity as well, as the efficiency of charge transfer and charge collection is known to be highly efficient.[14, 66]

2. Molecular excitonic states exhibit highly structured absorption spectra. Thus, to increase the photocurrent in organic PV, one must choose a combination of active materials that absorb evenly across the visible spectrum. In contrast, separating the optical and electrical functions allows the reaction center to be optimized at a single peak wavelength corresponding to the emission of the antenna.

3. Since the light absorbing antenna layer no longer needs to transport charge, new classes of solar cell materials can be used. The ideal antenna layer should be highly absorptive and have a high efficiency for photoluminescence (PL) such that reemission is strong. Candidate materials include those which absorb strongly like J-aggregates, nanometallic particles, quantum dots, and photosynthetic complexes that possess high quantum photoluminescent efficiency such as phycobilisomes from cyanobacteria and red algae. While quantum dots and nanometallic particles have been embedded as active layer of solar cells previously,[67, 68] their poor charge transport characteristics have decreased overall device performance.

4. The energetic funneling that biological antennas like cholorosomes employ can be utilized in mixed antenna layers. In mixed layers, light can be absorbed in a host material and energy is funneled to a less absorptive, highly luminescent material for reemission into the bound modes. By employing energetic funneling, broadband absorption can be achieved by judicious antenna design.

4.2 Absorption of SPP Excitation in Artificial Reaction Centers

The direct sensing of surface plasmon resonance via the transduction of the surface wave electric field enhancement in solar cells whose upper electrode composes of the active sensing element is a direct demonstration of the utility of SPP in the excitation of photovoltaic devices. Photocurrent enhancement in organic photodiodes under SPP excitation have been previously demonstrated [69, 70, 71, 72, 73, 74], but typical external quantum efficiencies peak at 0.05%.[70] In this case, a single layer copper phthalocyanine (CuPc)-Al Schottky diode exhibits a factor eight current enhancement at resonance attributed to increased absorption. In this work, a thin film organic photodiode is illuminated with $\lambda = 532\,\mathrm{nm}$ excitation in the Kretschmann geometry under attenuated total reflection (ATR); see figure 4-3. We observe a doubling in external quantum efficiency at SPP resonance over the normal illumination case. This represents a factor of 240 improvement in quantum efficiency over the previous cell. We achieved this improvement by utilizing a double heterojunction previously demonstrated to function well as a solar cell [63] with the materials CuPc, C_{60}, and bathocuproine (BCP), modified to consist of two Ag electrodes.

Double heterostructure organic photodiodes were fabricated on cleaned glass substrates. We purified the commercially available organic layers by thermal gradient sublimation prior to growth. Films were deposited at room temperature at high vacuum ($\sim 2 \times 10^{-6}\,\mathrm{Torr}$) in the following order: 15 nm silver, 14 nm of the donor-like material CuPc and 29 nm of the acceptor-like material C_{60}. Next, a 8 nm thick layer of BCP was grown; BCP has been previously shown to function as an exciton blocking, electron transport layer in both organic light emitting diodes [75] and solar cells [63]. This layer was followed by a 180Å thick layer of silver shadowmasked to define cathodes of $1.4 \times 10^{-2}\,\mathrm{cm}^2$. Light is coupled to the diode via a hemicylindrical prism attached to the glass substrate with index matching fluid. The prism and photodiode were mounted on a computer controlled rotating stage and illuminated with polarized light of wavelength $\lambda = 532\,\mathrm{nm}$ with an incident power intensity near 50

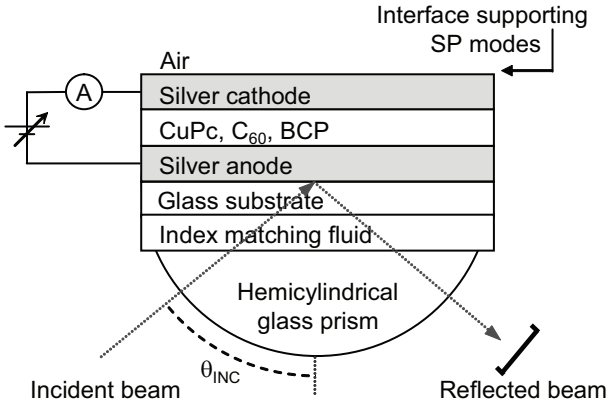

Figure 4-3: **Kretschmann experimental configuration** Monochromatic p-polarized laser light of wavelength 532 nm was illuminated onto a prism coupled to the glass substrate through index matching fluid. The device structure was glass/ Ag (23 nm)/ CuPc(14)/ C_{60}(34)/ BCP(8)/Ag (24).

µW. As the angle of incidence, θ_i, increases past the angle of total internal reflection, incident photons in the more optically dense glass substrate will resonantly excite surface plasmons on the Ag cathode-air interface. The intensity of the reflected beam is monitored with a Si photodetector. The measured photocurrent at zero bias is measured with a Keithley 2400 sourcemeter.

Reflection and net absorption of the electromagnetic wave were modeled using the transfer matrix method. Since the active material layers employed in our device structures have strong absorption peaks in the range of wavelengths we are considering, Stokes reversibility relations were not used in the calculation of the individual matrix elements. Indices of refraction and extinction coefficients for Ag [76, 77] and CuPc [8] were obtained from literature, while those for C_{60} and BCP were measured by spectroscopic ellipsometry. We used standard plane wave analysis to analyze the electric and magnetic fields in the multilayer structure.[78] The electric field in any layer j, is given for TM polarization by:

$$E_j = \left(A_{1j}e^{ik_{z,j}z}\left(1, 0, k_x/k_{z,j}\right) + A_{2j}e^{ik_{z,j}z}\left(1, 0, -k_x/k_{z,j}\right)\right)e^{i(k_x x - \omega t)} \qquad (4.1)$$

where k_x is the wavevector in the plane of the interfaces of the structure, calculated

from the incident beam. Imposition of boundary conditions at each interface leads to a set of equations for the coefficients A_j that are solved using transfer matrix methods. The magnetic fields in the structure can be calculated using the usual relation for electromagnetic waves. This enables the calculation of the Poynting vector in each layer of the structure.

In figure 4-4a we compare proportional reflected light intensity (reflectivity) versus θ_i for both s- and p-polarized incident light. The mixed transversal and longitudinal electromagnetic field carried by SPPs can only be excited by p-polarized light and as such, only the p-polarized reflectivity exhibits a sudden decrease corresponding to SPP excitation.[79] As θ_i increases, the onset of attenuated total reflection at 44° excites an evanescent surface wave which couples to SPPs on the Ag cathode-air interface. Photonic excitation of SPs via prism coupling also allows radiative re-emission of light back into the glass hemicylinder. This back scattered light is 180° out of phase with the incident light; at resonance this backscattered light can destructively interfere with the incoming wave resulting in the sharp drop in reflectivity observed surface plasmon resonance (SPR).

The modeled reflectivity spectra is a strong function of the thickness and complex permittivity of the two layers whose interface support the surface wave. We modeled surface roughness applying the method of Hornauer [77] as a perturbation of the permittivity of a 'smooth' silver film. We have measured rms roughness parameters by atomic force microscopy for the scattering silver films to be ~ 1.5 nm and adjust the index of refraction n and extinction coefficient k in accordance with Hornauer, yielding $n = 0.14$ and $k = 2.56$, significantly broadening the reflectivity dip and shifting the resonance to higher momentum.

Besides the back-radiation damping of SPPs at the Ag-air interface, the surface wave vector of the SPP can linearly combine with the vectors which compose the Fourier spectrum of the rough surface. These scattering events allow the non-radiative SPPs to forward scatter photons in the dielectric (air) at the interface of field enhancement. The correlation between surface roughness and directional light emission has been measured by several authors. [80, 81, 82] According to Tajima et al.,[82] the

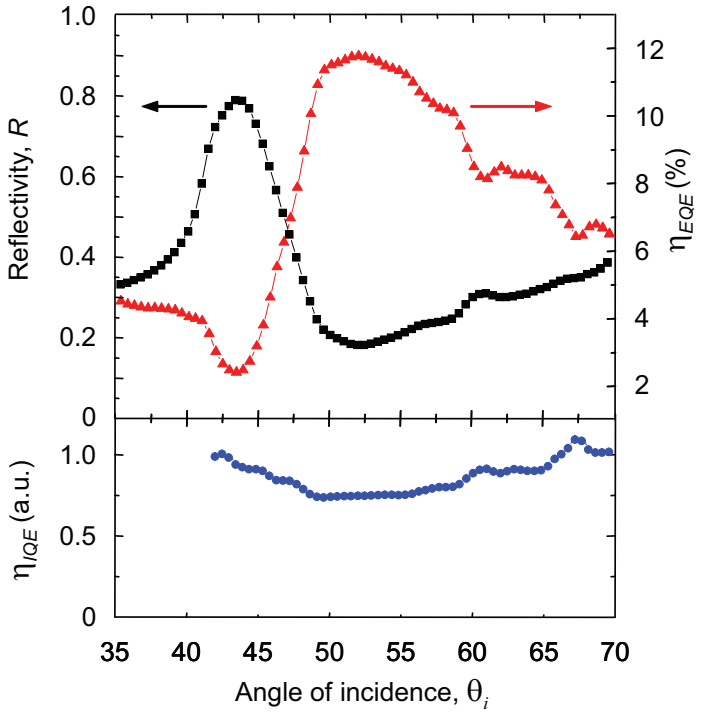

Figure 4-4: **Reflectivity and quantum efficiency of SPP excited photodiode** (a) Maximum coupling of light to SPPs occurs where the reflected optical intensity (■) is a minimum and the photodiode external quantum efficiency (▲) is a maximum at $\sim 53°$, where the external quantum efficiency is 12%. (b) Internal QE as a function of incident angle (•), where the $A = 1 - R$. The spectra was normalized at $\theta_i = 35°$.

efficiency of light emission from films of 1.5 nm rms roughness is $\sim 10\%$.

The electromagnetic field of the SPPs excite electron-hole pairs at the Fermi level of the silver; the following de-excitation produces phonons and thus heating. The internal damping of SPPs by joule heating is least of the noble metals for Ag; δ_{SP}^{Ag} at 532 nm is $\sim$ 30µm. The increase in interaction distance of photodiodes excited parallel to the device interface instead of perpendicular is a factor of 600. This represents a substantial increase, greatly increasing light absorption and thus improving quantum efficiency.

In figure 4-4a the measured external quantum efficiency (QE) is plotted versus θ_i, showing a tripling of quantum efficiency from normal incidence (approximated here by $\theta_i = 35°$) from 4.3% to 12%, due to an increase in η_{ABS} under SPP excitation. The external QE, η_{EQE}, is related to internal QE, η_{IQE}, by $\eta_{EQE} = \eta_{ABS} \cdot \eta_{IQE}$. The total

absorption in the multilayer stack is $A \approx 1 - R - T$. We approximate $A \approx 1 - R$ by letting $T = 0$ which is exact only under the condition of total internal reflection where the angle of incidence is greater than the angle of SP resonance, $\theta_i > \theta_{SPR}$. Below θ_{SPR}, transmission is small but nonzero. Under this approximation, the normalized angular dependence of η_{IQE} is plotted in figure 4-4b. Despite the doubling of η_{EQE} under SPP excitation, η_{IQE} is nearly flat both below and above $\theta_i = 44°$ where the transition between excitation via photons and SPPs occurs. The maximum reduction is $\sim$ 25% at $\theta = 50°$, attributable to increased absorption in the silver cathode that supports the plasmon and outscattering of light, processes exacerbated by surface roughness at the electrode-air interface.[79] Since the normalized η_{IQE} is nearly flat coupling between SPPs and the organic layers is efficient.

Disparities between η_{EQE} and η_{ABS} as a function of θ_i is attributable to two phenomena associated with SPP propagation on metal surfaces. First, as the angle of incidence is increased, more light energy is guided into SPP modes. At plasmon resonance, energy dissipation reaches a maximum, resulting in a decrease in internal QE. Second, light emission associated with propagating SPPs results in the outcoupling of useful energy. Both phenomena compete with light absorption in the artificial reaction center and constitute loss.

If we assume that the modeled η_{ABS} provides an accurate prediction of absorption versus θ_i, η_{IQE} is estimated to be $\sim$ 20%. This value is low but has been shown to be highly dependent on exposure to air and attributable to device degradation.[83] However, in absorption limited devices, the thickness of the active absorbing layers can be made thinner, which has previously been shown to significantly increase η_{IQE} by increasing the probability of exciton dissociation at the active interface [82]. Active semiconductor layers with thicknesses greater than the exciton diffusion length lowers dissociation efficiency. We expect that the demonstrated photodiode can achieve higher QEs under device structure optimization.

The modeled total electric field intensity throughout the thickness dimension is shown in figure 4-5 for θ_i at 30° and 47°. The field enhancement at the Ag-air interface is consistent with the SPP propagation and is the only possible mode ex-

citable through the prism coupled Kretschmann geometry. For incident radiation with $\lambda = 532\,\mathrm{nm}$, absorption is primarily in the CuPc layer. Total absorption is calculable by integrating the divergence of the Poynting vector $\overrightarrow{S}$ across the thickness of interest. At SPR, over 80% of absorbed light is absorbed in the CuPc layer. However, the CuPc layer is 40 nm from the Ag-air interface. A stronger field enhancement is possible with decreasing distance from the SP supporting interface and will result in greater absorption.

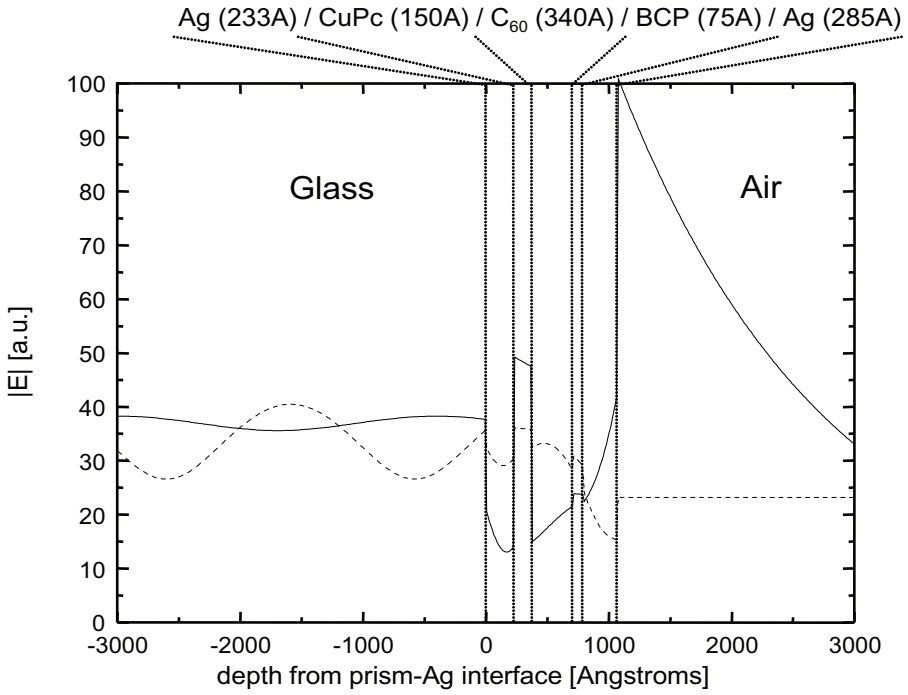

Figure 4-5: **Magnitude of the electric field in SPP excited photodiode** A pronounced enhancement at the silver-air interface indicates plasmon resonance. The fields in the absorbing artificial reaction center are also enhanced, leading to an increase in external quantum efficiency.

Photon launched surface plasmon excitation of organic photodiodes demonstrates that the efficiency of artificial reaction centers is enhanced when the incident radiation is coupled into a guided SPP mode. The enhancement of efficiency is most pronounced for thin reaction centers, with low exciton diffusion losses and low optical absorption, but very high internal quantum efficiency. SPP excitation in the

Kretschmann configuration resulting in internal QEs that are independent of excitation method suggests SPP excitation of artificial reaction centers can proceed with high efficiency.

4.3 Energy Transfer from Synthetic Antennas to Synthetic Reaction Centers

4.3.1 Simulation of Energy Transfer from Antenna Excitons

Energetic transfer from excited molecules to SPP modes can occur with high efficiency to metallic slabs [84, 85] and thin films.[86] The theoretical basis for dipole coupling to modes in a multilayer stack is well understood [87] and agrees well with experiments.[88] To examine dipole coupling to thin silver films comprising the cathode of an organic PV, we use the method of Chance et al. [87] to simulate classical damping of an oscillating charge distribution near a multilayer stack to investigate energy transfer to our artificial reaction center. Energy transfer is calculated directly from the Poynting vector.[89]

In figure 4-6, we show the dispersion relation for guided SPP modes, propagating parallel to the electrode plane in a typical photovoltaic cell with external antenna. Three guided modes are identified in this structure and the mode intensity profile of each is shown in the insets. Each of the guided modes has significant overlap with the charge generation layers sandwiched between the metal electrodes. The mode labeled (a), the SPP centered on the silver/reaction center interface, has by far the highest intensity in the antenna.

We calculate the dipole energy dissipation to the multilayer stack in a technologically relevant device geometry as a function of normalized wavevector, u, and distance to the antenna-silver layer interface in figure 4-7. The normalization factor for the wavevector is its free space value; normalized wavevectors with $u < 1$, correspond to radiative modes; $u > 1$ correspond to non-radiative energy transfer. Since the energy coupling is dependent on the transition dipole orientation with respect to the plane

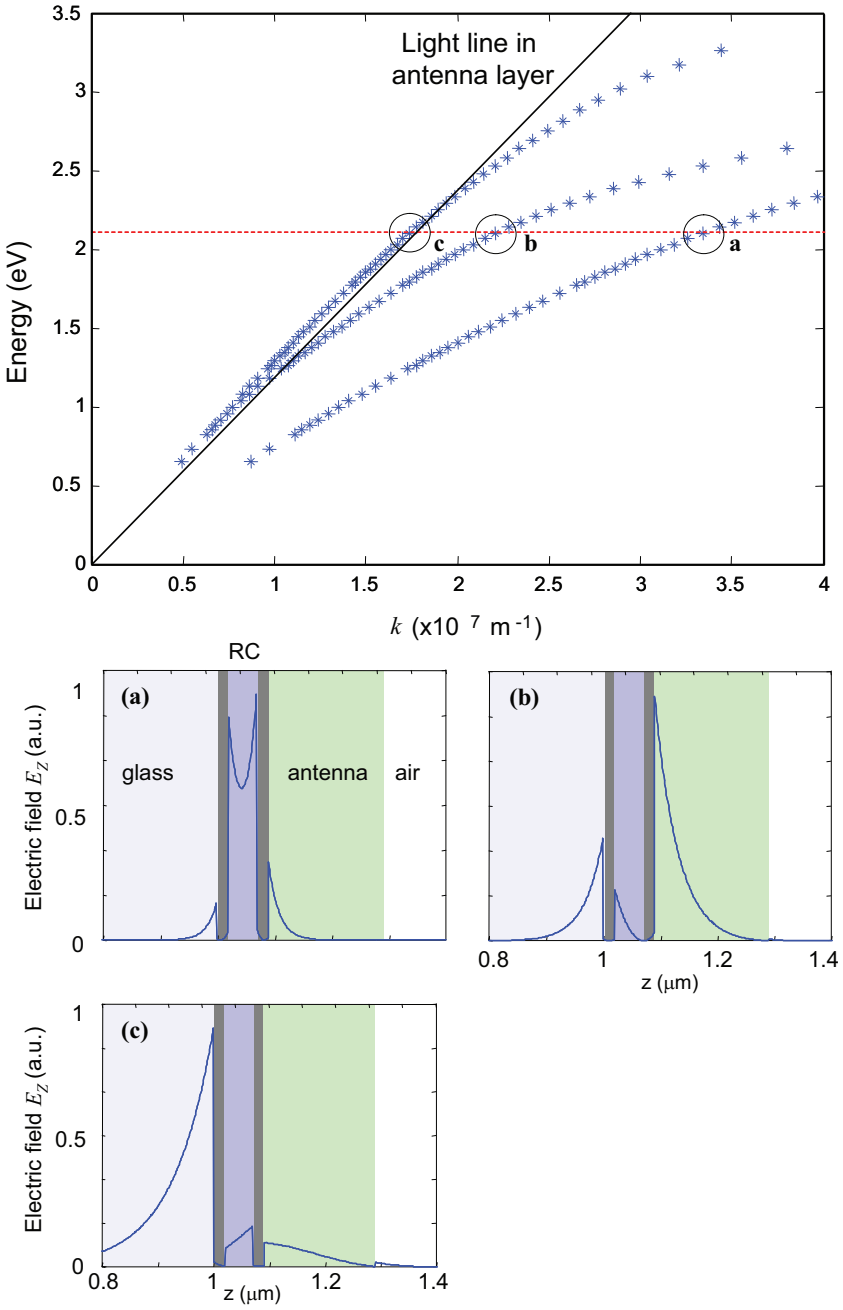

Figure 4-6: **Surface plasmon polariton mode dispersion and field profile in an organic solar cell** (a) Calculated dispersion relation of modes in the multilayer stack. The curves correspond to SPP modes shifted to the right of the photon dispersion light lines in the dielectrics that partially support the SPP. The electric field profile in the thickness direction for $E = 2.1\,\text{eV}$ shows the field localization at the interfaces that support the SPP modes. Mode (a) is strongest in the reaction center semiconductor. Mode (b) is strongest in the antenna, and Mode (c) is strongest in the glass substrate. Because it has the highest intensity in the antenna, mode (b) dominates energy transfer from the antenna to the RC. The structure of the simulated device is: glass/ Ag(20 nm)/ CuPc(45)/ PTCBI(25)/ BCP(13)/ Ag(30)/ air.

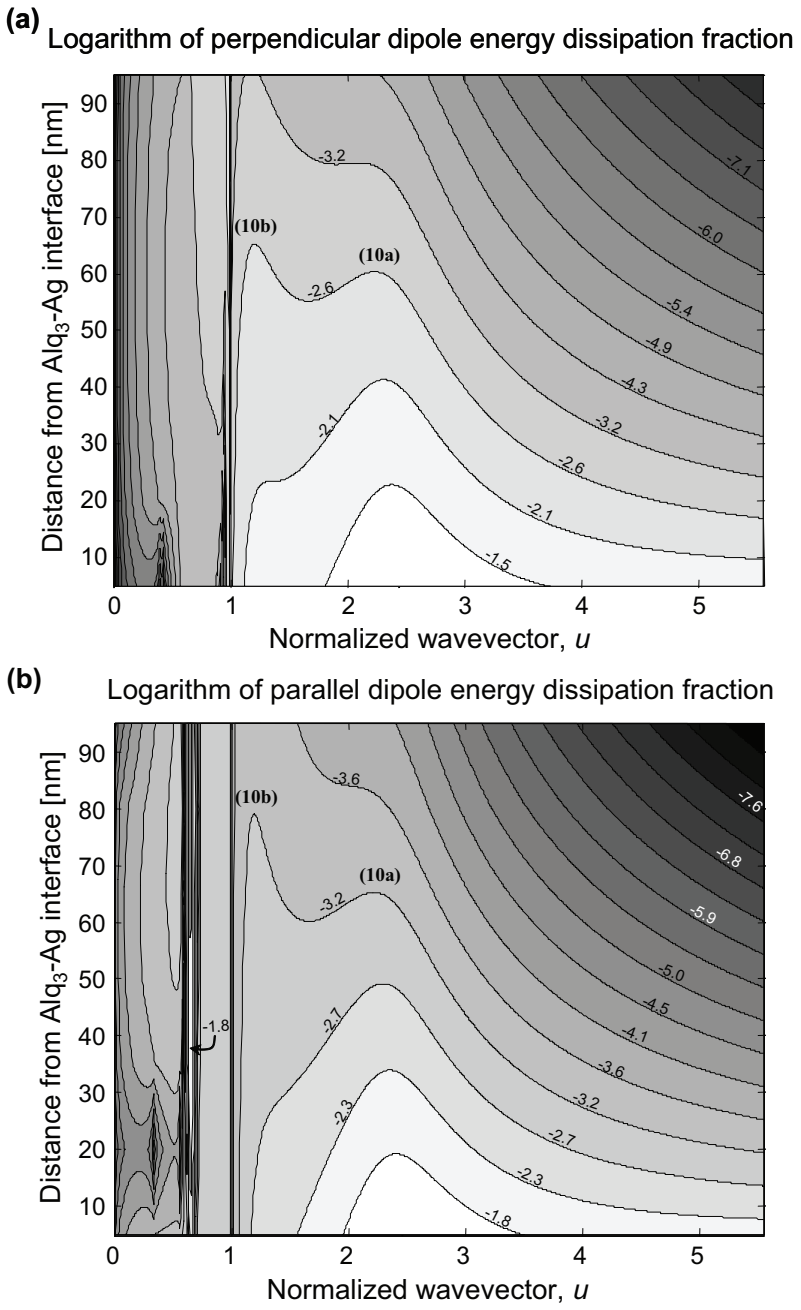

Figure 4-7: **Logarithmic contour plot of dipole energy dissipation in an artificial antenna dipole** for (a) perpendicular and (b) parallel orientation. The peaks labeled (10a) and (10b) correspond to the guided modes in figure 4-2. Dipole energy dissipation is greatest for perpendicularly oriented dipoles into modes with $u > 1$, corresponding to SPPs. Also, note that coupling to waveguide modes is strongest for dipoles oriented parallel to the Ag-antenna interface. The structure modeled here is air/ Alq_3(210 nm)/ Ag(15)/ BCP(10)/ PTCBI(20)/ CuPc(30)/ Ag(45)/ glass. The photoluminescent wavelength, λ, and free space quantum efficiency, q, of the dipole are 650 nm and 70%, respectively. Energy dissipation is plotted as a logarithm to facilitate visual interpretation.

of the interface, we consider the cases of perpendicular (figure 4-7a) and parallel (figure 4-7b) orientation separately. At a given dipole distance, integration of the energy dissipation yields unity. If the molecules are randomly oriented, the transition dipoles will be 1/3 perpendicular and 2/3 parallel.

Energy transfer to the stack confirms that of the four decay mechanisms listed above, guided electromagnetic modes are dominant. For perpendicularly oriented dipoles (figure 4-6a), prevailing energy transfer is to the non-radiative SPP modes with normalized propagation constant $u = 1.2$. This corresponds to mode (a) in figure 4-5. Mode (b) is also visible but much weaker. The non-radiative character ($u > 1$) of these modes describes their interfacial localization. Coupling to SPPs is especially strong near the interface, as expected. For dipoles parallel to the interface, both waveguide and SPPs modes are significant. The waveguided photon modes exist in the antenna layer, where the nodes are set by the reflection conditions at the adjacent silver layer and the neighboring air interface for the condition of total internal reflection. For the structure modeled here, only the primary mode exists, however the number of modes increases as the luminescence wavelength of the dipole decreases and/or the antenna thickness increases.

The efficiency of energy transfer from the antenna to the active layers within the reaction center is shown in figure 4-8 for various dipole orientations. The efficiency was calculated directly from the Poynting vector. The structure is glass / Ag(25 nm) / RC (50, modeled by copper phthalocyanine, CuPc) / Ag(25)/ antenna (200, $n = 1.7$)/ air. We also assume an antenna with a free space photoluminescent efficiency of 70% and emission at $\lambda = 620\,\text{nm}$. For antennas comprised of molecules with isotropic transition dipole moments, the efficiency of energy transfer to the RC is typically greater than 50%.[1]

[1]Note that molecules with transition dipoles oriented perpendicularly absorb the least incident radiation. The ideal antenna should transfer energy from parallel dipoles, which have the highest absorption, to perpendicular dipoles.

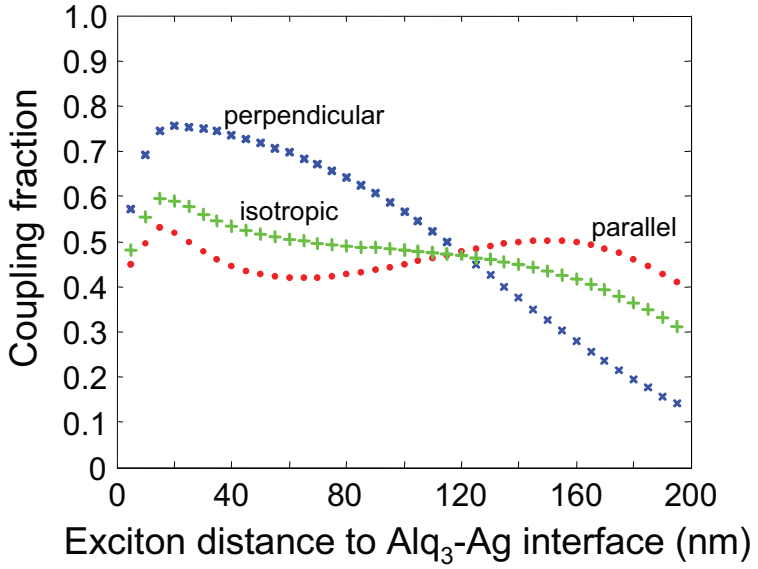

Figure 4-8: **Efficiency of energy transfer from excitons in the antenna to the RC as a function of the exciton position and orientation in the antenna** The structure modeled here is glass/Ag(25 nm)/ RC(50, modeled by copper phthalocyanine, CuPc)/ Ag(25)/ antenna(200, $n = 1.7$)/ air. The photoluminescent wavelength, λ , and free space quantum efficiency, q, of the dipole are 620 nm and 70%, respectively.

4.3.2 Experimental Verification of Energy Transfer from Antenna Excitons to Surface Modes

Finally, we experimentally demonstrate energy transfer from the antenna in figure 4-9. In this experiment we fabricated devices with two different artificial antennas. The first employed a 200 nm-thick co-deposited film of tris(8-hydroxyquinoline) aluminum (Alq_3) and 1% DCM2. In the second antenna, the Alq_3 was instead doped with 1% CuPc. In both antennas, light is absorbed in the blue and near UV by Alq_3 molecules, which then transfer that energy to the dopant guest molecules. Photoluminescence (PL) into surface modes then occurs from the dopants. However, the PL efficiency for DCM2 is approximately 70%, whereas for CuPc it is nearly 0%, prohibiting energy transfer to the artificial reaction center. By comparing the quantum efficiency spectra of these two devices, we can attribute positive deviations to energy transfer.

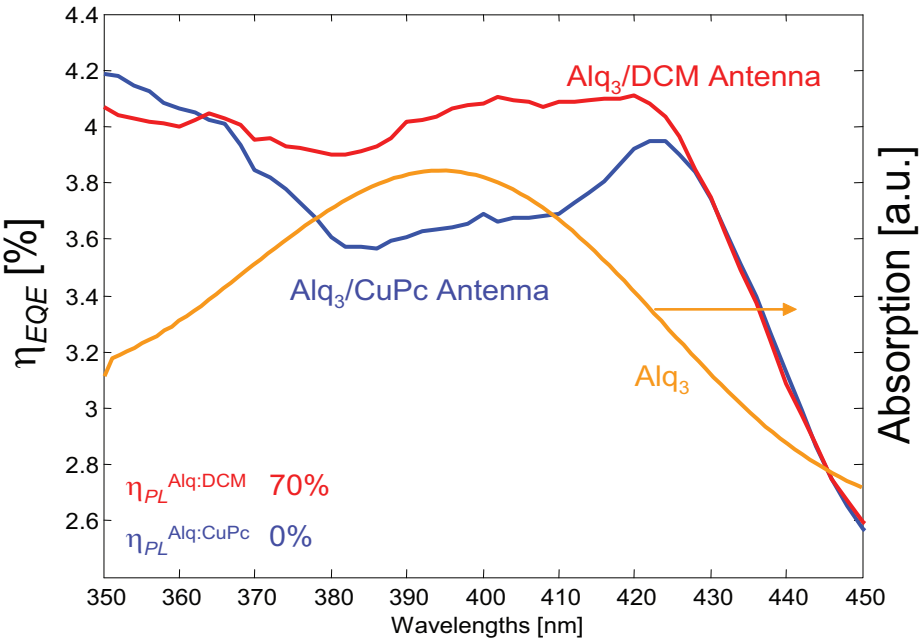

Figure 4-9: **Quantum efficiency spectra of artificial antenna solar cells** The photocurrent spectra of PV cells with external Alq_3-based antennas show enhanced photocurrent at wavelengths where Alq_3 absorbs. An increase in quantum efficiency for the Alq_3:DCM2 antenna coincides with the absorption maximum of Alq_3, demonstrating energy coupling from the artificial antenna to artificial reaction center. The device structure is Ag(20 nm)/ CuPc(40)/ PTCBI(20)/ BCP(10)/ Ag(30)/ Antenna(200).

The complete structure of the solar cell here is Ag(20 nm)/ CuPc(40)/ PTCBI(20)/ BCP(10)/ Ag(30)/ Antenna(200). For wavelengths above $\lambda = 450\,\text{nm}$, the quantum efficiency spectra are nearly identical, showing that the antenna doesn't perturb the diode performance at frequencies where the antenna is inactive. However, the efficiency exhibits a modest increase around $\lambda = 390\,\text{nm}$, corresponding to the Alq_3 absorption peak. The correlation between an increased photoluminescence quantum efficiency and increased external quantum efficiency, localized to the narrow absorption peak of the antenna, demonstrates that energy coupling from the antenna layer has occurred. The quantum efficiency is low overall since the antenna-less solar cell suffers from a low internal quantum efficiency. Higher efficiencies are possible by improving the efficiency of the reaction center.

Chapter 5

Conclusion

Photosynthetic structures are attractive for implementation in organic PV due to their highly efficient functioning while in their native environments. Device performance of the first demonstrations of solid state solar cells with integrated photosynthetic proteins are limited, as are traditional organic solar cells, by an inability to absorb enough incident light. This problem is endemic to thin films of even strongly absorbing materials and constitutes a limitation that must be addressed with alternative techniques.

The local environment of the solid state is drastically different to the aqueous solution where proteins usually preside. Since the structural stability and hence functionality of proteins hinges on local environment, it is necessary to inquire whether the harsh environment of solid matter is too destructive for proteins to withstand. We find that solid state integration necessitates stabilization by surfactants and have demonstrated retained functionality over the timescale of weeks. To be useful in practical devices, significant work in increasing stability is needed. The stability of photosynthetic reaction centers are compromised even in their native thylakoid membranes; the half-life of PSII can be as short as 30 minutes.[90] Plants survive this damage through an energetically costly and complicated repair process of degrading, resynthesis, and replacement.

Separation of the functions of light absorption and exciton dissociation constitutes a significant photosynthetic redesign, unaccompanied by the limitations of traditional

organic PV. Initial device performances are modest yet promising. The separation of optical and electrical functionalities discussed here represents a completely synthetic implementation where the active materials of the artificial antenna and reaction center are amorphous films of pigment semiconductors. However, it is possible to construct devices where one or both components are biological in origin. The excellent absorption characteristics of chlorosomes and charge separation characteristics of reaction centers make them tempting candidates for photovoltaic materials, the tradeoff between performance and stability may dictate which type of devices yield high performance and reliability.

Bibliography

[1] Sheats, J. R. Manufacturing and commercialization issues in organic electronics. *Journal of Materials Research* **19**, 1974–1989 (2004).

[2] McKeown, N. B. *Phthalocyanine materials: synthesis, structure, and function.* Chemistry of solid state materials ; 6 (Cambridge University Press, Cambridge, U.K. ; New York, 1998).

[3] Wohrle, D. Phthalocyanines in macromolecular phases - methods of synthesis and properties of the materials. *Macromolecular Rapid Communications* **22**, 68–97 (2001).

[4] Xue, J. G., Uchida, S., Rand, B. P. & Forrest, S. R. Asymmetric tandem organic photovoltaic cells with hybrid planar-mixed molecular heterojunctions. *Applied Physics Letters* **85**, 5757–5759 (2004).

[5] Li, G. *et al.* High-efficiency solution processable polymer photovoltaic cells by self-organization of polymer blends. *Nature Materials* **4**, 864–868 (2005).

[6] Green, M. A., Emery, K., King, D. L., Hisikawa, Y. & Warta, W. Solar cell efficiency tables - (version 27). *Progress in Photovoltaics: Research and Applications* **14**, 46–51 (2006).

[7] of Energy, U. D. Basic research needs for solar energy utilization. Tech. Rep. (2005).

[8] Peumans, P., Yakimov, A. & Forrest, S. R. Small molecular weight organic thin-film photodetectors and solar cells. *Journal of Applied Physics* **93**, 3693–3723 (2003).

[9] Pope, M. & Swenberg, C. *Electronic Processes in Organic Crystals* (Oxford University Press, Oxford, 1982), 1st edn.

[10] Silinsh, E. A. & Capek, V. *Organic Molecular Crystals: Interaction, Localization, and Transport Phenomena* (AIP Press, New York, 1994).

[11] Zerza, G., Brabec, C. J., Cerullo, G., De Silvestri, S. & Sariciftci, N. S. Ultrafast charge transfer in conjugated polymer-fullerene composites. *Synthetic Metals* **119**, 637–638 (2001).

[12] Forrest, S. R. The limits to organic photovoltaic cell efficiency. *Mrs Bulletin* **30**, 28–32 (2005).

[13] Gratzel, M. Solar energy conversion by dye-sensitized photovoltaic cells. *Inorganic Chemistry* **44**, 6841–6851 (2005).

[14] Peumans, P., Uchida, S. & Forrest, S. R. Efficient bulk heterojunction photovoltaic cells using small-molecular-weight organic thin films. *Nature* **425**, 158–162 (2003).

[15] Huynh, W. U., Dittmer, J. J. & Alivisatos, A. P. Hybrid nanorod-polymer solar cells. *Science* **295**, 2425–2427 (2002).

[16] Coakley, K. M. & McGehee, M. D. Photovoltaic cells made from conjugated polymers infiltrated into mesoporous titania. *Applied Physics Letters* **83**, 3380–3382 (2003).

[17] Law, M., Greene, L. E., Johnson, J. C., Saykally, R. & Yang, P. D. Nanowire dye-sensitized solar cells. *Nature Materials* **4**, 455–459 (2005).

[18] Purves, W. K. *Life, the science of biology* (Sinauer Associates ; W.H. Freeman and Co., Sunderland, Mass. Gordonsville, VA, 2004), 7th edn.

[19] Green, B. & Parson, W. *Light-Harvesting Antennas in Photosynthesis*, vol. 13 of *Advances in Photosynthesis and Respiration* (Kluwer Academic, Dordrecht, 2003).

[20] Psencik, J. *et al.* Lamellar organization of pigments in chlorosomes, the light harvesting complexes of green photosynthetic bacteria. *Biophysical Journal* **87**, 1165–1172 (2004).

[21] Mukhopadhyay, B., Johnson, E. F. & Ascano, M. Conditions for vigorous growth on sulfide and reactor-scale cultivation protocols for the thermophilic green sulfur bacterium chlorobium tepidum. *Applied and Environmental Microbiology* **65**, 301–306 (1999).

[22] Matsuura, K., Hirota, M., Shimada, K. & Mimuro, M. Spectral forms and orientation of bacteriochlorophyll-c and bacteriochlorophyll-a in chlorosomes of the green photosynthetic bacterium chloroflexus-aurantiacus. *Photochemistry and Photobiology* **57**, 92–97 (1993).

[23] Holzwarth, A. R. & Schaffner, K. On the structure of bacteriochlorophyll molecular aggregates in the chlorosomes of green bacteria - a molecular modeling study. *Photosynthesis Research* **41**, 225–233 (1994).

[24] Nozawa, T. *et al.* Structures of chlorosomes and aggregated bchl-c in chlorobium-tepidum from solid-state high-resolution cp/mas c-13 nmr. *Photosynthesis Research* **41**, 211–223 (1994).

[25] Novoderezhkin, V. I. & Fetisova, Z. G. Oligomerization of light-harvesting pigments as a structural factor optimizing the photosynthetic antenna function .3. model of oligomeric pigment organization in antennae of green bacteria. *Molecular Biology* **31**, 435–440 (1997).

[26] van Rossum, B. J. *et al.* A refined model of the chlorosomal antennae of the green bacterium chlorobium tepidum from proton chemical shift constraints ob-

tained with high-field 2-d and 3-d mas nmr dipolar correlation spectroscopy. *Biochemistry* **40**, 1587–1595 (2001).

[27] Dimitrakopoulus, C. D., Brown, A. R. & Pomp, A. Molecular beam deposited thin films of pentacene for organic field effect transistor applications. *Journal of Applied Physics* **80**, 2501–2508 (1996).

[28] Fraxedas, J. Perspectives on thin molecular organic films. *Advanced Materials* **14**, 1603–1614 (2002).

[29] Shtein, M. S., Mapel, J. K., Benziger, J. B. & Forrest, S. R. Effects of film morphology and gate dielectric surface preparation on the electrical characteristics of organic-vapor-phase-deposited pentacene thin-film transistors. *Applied Physics Letters* **81**, 268–270 (2002).

[30] Witte, G. & Woll, C. Growth of aromatic molecules on solid substrates for applications in organic electronics. *Journal of Materials Research* **19**, 1889–1916 (2004).

[31] Blankenship, R. *Molecular Mechanisms of Photosynthesis* (Blackwell Science, Oxford, 2002), 1 edn.

[32] Hoff, A. & Deisenhofer, J. Photophysics of photosynthesis. *Physics Reports* **287**, 1–247 (1997).

[33] Humphrey, W., Dalke, A. & Schulten, K. Vmd - visual molecular dynamics. *J. Molec. Graphics* **14**, 33–38 (1996).

[34] Bolton, J. R. & Hall, D. O. Photochemical conversion and storage of solar energy. *Annual Review of Energy* **4**, 353–401 (1979).

[35] Hall, D. O. & Rao, K. K. *Photosynthesis* (Cambridge University Press, Cambridge, 1999), 6th edn.

[36] Wurfel, P. *Physics of Solar Cells* (Wiley VCH, Weinheim, 2005).

[37] Montano, G. A. *et al.* Characterization of chlorbium tepidum chlorosomes: a calculation of bacteriachlorophyll c per chlorosomes and oligomer modeling. *Biophysical Journal* **85**, 2560 (2003).

[38] Sussman, A. Space-charge-limited currents in copper phthalocyanine thin films. *Journal of Applied Physics* **38**, 2738–2748 (1967).

[39] Cassida, K. A. *et al.* Biomass yield and stand characteristics of switchgrass in south central u.s. environments. *Crop Science* **45**, 673–680 (2005).

[40] Byrd, G. T. & May II, P. A. Physiological comparisons of switchgrass cultivars differing in transpiration efficiency. *Crop Science* **40**, 1271–1277 (2000).

[41] Walker, D. *Energy, Plants and Man* (Oxygraphics, Brighton, 1992).

[42] Tang, C. W. & Albrecht, A. C. Photovoltaic effects of metal-chlorophyll-a-metal sandwhich cells. *Journal of Chemical Physics* **62**, 2139–2149 (1975).

[43] Katz, E. Application of bifunctional reagents for immobilization of proteins on a carbon electrode surface: oriented immobilization of photosynthetic reaction centers. *Journal of Electroanalytical Chemistry* **365**, 157–164 (1994).

[44] Trammell, S. A., Wang, L., Zullo, J. M., Shashidhar, R. & Lebedev, N. Oriented binding of photosynthetic reaction centers on gold using ni-nta self-assembled monolayers. *Biosensors and Bioelectronics* **19**, 1649–1655 (2004).

[45] Smith, M., Furman, T., Ingolia, T. & Pidgeon, C. Chelating peptide-immobilized metal ion affinity chromatography. a new concept in affinity chromatography for recombinant proteins. *Journal of Biological Chemistry* **263**, 7211–7215 (1988).

[46] Moore, M. H., Trammell, S. A., Pollack, S. K., Lebedev, N. & Kushmerick, J. G. Optimizing charge transfer between photosynthetic proteins and electrode surfaces. *Abstracts of Papers of the American Chemical Society* **229**, U664–U664 (2005).

[47] Lee, I., Lee, J. W. & Greenbaum, E. Biomolecular electronics: Vectorial arrays of photosynthetic reaction centers. *Physical Review Letters* **79**, 3294–3297 (1997).

[48] Minai, L., Fish, A., Darash-Yahana, M., Verchovsky, L. & Nechushtai, R. The assembly of the psad subunit into the membranal photosystem i complex occurs via an exchange mechanism. *Biochemistry* **40**, 12754–12760 (2001).

[49] Cleveland, J., Anczykowski, B., Schmid, A. & Elings, V. Energy dissipation in tapping-mode atomic force microscopy. *Applied Physics Letters* **72**, 2613–2615 (1998).

[50] Das, R. *et al.* Solid state integration of photosynthetic protein molecular complexes. *Nano Letters* **4**, 1079–1083 (2004).

[51] Renger, T., May, V. & Kuhn, O. Ultrafast excitation energy transfer dynamics in photosynthetic pigment-protein complexes. *Physics Reports* **343**, 137–254 (2001).

[52] Kiley, P. *et al.* Self-assembling peptide detergents stabilize isolated photosystem i on a dry surface for an extended time. *PLoS Biology* **3**, e230 (2005).

[53] Mi, Y., Wood, G., Thoma, L. & Rashed, S. Effects of polyethylene glycol molecular weight and concentration of lactate dehydrogenase activity in solution and after freeze-thawing. *PDA Journal of Pharmaceutical Science and Technology* **56**, 115–123 (2002).

[54] Vauthey, S., Santoso, S., Gong, H., Watson, N. & Zhang, S. Molecular self-assembly of surfactant-like peptides to form nanotubes and nanovesicles. *Proceedings of the National Academy of Sciences of the United States of America* **99**, 5355–5360 (2002).

[55] Santoso, S., Hwang, W., Hartman, H. & Zhang, S. Self-assembly of surfactant-like peptides with variable glycine tails to form nanotubes and nanovesicles. *Nano Letters* **2**, 687–691 (2002).

[56] von Maltzahn, G., Vauthey, S., Santoso, S. & Zhang, S. Positively charged surfactant-like peptides self-assemble into nanostructures. *Langmuir* **19**, 4332–4337 (2003).

[57] Zhang, S. Fabrication of novel biomaterials through molecular self-assembly. *Nature Biotechnology* **21**, 1171–1178 (2003).

[58] Morosinotto, T., Breton, J., Bassi, R. & Croce, R. The nature of a chlorophyll ligand in lhca proteins determines the far red fluorescence emission typical of photosystem i. *Journal of Biological Chemistry* **278**, 49223–49229 (2003).

[59] Wang, P. *et al.* A stable quasi-solid-state dye-sensitized solar cell with an amphiphilic ruthenium sensitizer and polymer gel electrolyte. *Nature Materials* **2**, 402–407 (2003).

[60] Barber, J. & Andersson, B. Revealing the blueprint of photosynthesis. *Nature* **370**, 31–34 (1994).

[61] Dutton, G. & Zhou, X.-Y. Unoccupied states in c60 thin films probed by two-photon photoemission. *Journal of Physical Chemistry B* **106**, 5975–5981 (2002).

[62] Hill, I. & Kahn, A. Organic semiconductor heterointerfaces containing bathocuproine. *Journal of Applied Physics* **86**, 4515–4519 (1999).

[63] Peumans, P. & Forrest, S. Very-high-efficiency double-heterostructure copper phthalocyanine/c60 photovoltaic cells. *Applied Physics Letters* **79**, 126–128 (2001).

[64] Straley, S. C., Parson, W. W., Mauzerall, D. C. & Clayton, R. K. Pigment content and molar extinction coefficients of photochemical reaction centers from rhodopseudomonas sphaeroides. *Biochimica et Biophysica acta* **305**, 597–609 (1973).

[65] Barnes, W. L., Dereux, A. & Ebbesen, T. W. Surface plasmon subwavelength optics. *Nature* **424**, 824–830 (2003).

[66] Brabec, C. J. *et al.* Tracing photoinduced electron transfer process in conjugated polymer/fullerene bulk heterojunctions in real time. *Chemical Physics Letters* **340**, 232–236 (2001).

[67] Rand, B. P., Peumans, P. & Forrest, S. R. Long-range absorption enhancement in organic thin-film solar cells containing silver nanoclusters. *Journal of Applied Physics* **96**, 7519–7526 (2004).

[68] Sargent, E. H. Infrared quantum dots. *Advanced Materials* **17**, 515–522 (2005).

[69] Kume, T., Hayashi, S., Ohkuma, H. & Yamamoto, K. Enhancement of photoelectric conversion efficiency in copper phthalocyanine solar cell: White light excitation of surface plasmon polaritons. *Japanese Journal of Applied Physics Part 1-Regular Papers Short Notes & Review Papers* **34**, 6448–6451 (1995).

[70] Kume, T., Hayashi, S. & Yamamoto, K. Enhancement of photoelectric conversion efficiency in copper phthalocyanine solar-cell by surface-plasmon excitation. *Japanese Journal of Applied Physics Part 1-Regular Papers Short Notes & Review Papers* **32**, 3486–3492 (1993).

[71] Hayashi, S., Kozaru, K. & Yamamoto, K. Enhancement of photoelectric conversion efficiency by surface-plasmon excitation - a test with an organic solar-cell. *Solid State Communications* **79**, 763–767 (1991).

[72] Wakamatsu, T., Saito, K., Sakakibara, Y. & Yokoyama, H. Enhanced photocurrent in organic photoelectric cells based on surface-plasmon excitations. *Japanese Journal of Applied Physics Part 2-Letters* **34**, L1467–L1469 (1995).

[73] Wakamatsu, T., Saito, K., Sakakibara, Y. & Yokoyama, H. Surface plasmon-enhanced photocurrent in organic photoelectric cells. *Japanese Journal of Applied Physics Part 1-Regular Papers Short Notes & Review Papers* **36**, 155–158 (1997).

[74] Kato, K. *et al.* Enhancement of optical absorption and photocurrents in solar cells of merocyanine langmuir-blodgett films utilizing surface plasmon excitations.

Materials Science & Engineering C-Biomimetic and Supramolecular Systems **22**, 251–256 (2002).

[75] Parthasarathy, G., Adachi, C., Burrows, P. E. & Forrest, S. R. High-efficiency transparent organic light-emitting devices. *Applied Physics Letters* **76**, 2128–2130 (2000).

[76] Johnson, P. B. & Christy, R. W. Optical-constants of noble-metals. *Physical Review B* **6**, 4370–4379 (1972).

[77] Hornauer, D. L. Light-scattering experiments on silver films of different roughness using surface plasmon excitation. *Optics Communications* **16**, 76–79 (1976).

[78] Morozov, G. V., Maev, R. G. & Drake, G. W. F. Multiple reflection method for electromagnetic waves in layered dielectric structures. *Quantum Electronics* **31**, 767–773 (2001).

[79] Raether, H. *Surface plasmons on smooth and rough surfaces and on gratings.* Springer tracts in modern physics ; 111 (Springer-Verlag, Berlin, 1987).

[80] Inagaki, T., Kagami, K. & Arakawa, E. T. Photo-acoustic study of surface-plasmons in metals. *Applied Optics* **21**, 949–954 (1982).

[81] Moreland, J., Adams, A. & Hansma, P. K. Efficiency of light-emission from surface-plasmons. *Physical Review B* **25**, 2297–2300 (1982).

[82] Tajima, H., Haraguchi, M. & Fukui, M. Surface-plasmon polariton radiation from silver films on fluoride films and surface-roughness parameters of those silver films. *Surface Science* **323**, 282–287 (1995).

[83] Peumans, P. & Forrest, S. R. Very-high-efficiency double-heterostructure copper phthalocyanine/c-60 photovoltaic cells (vol 79, pg 126, 2001). *Applied Physics Letters* **80**, 338–338 (2002).

[84] Weber, W. H. & Eagen, C. F. Energy-transfer from an excited dye molecule to the surface-plasmons of an adjacent metal. *Optics Letters* **4**, 236–238 (1979).

[85] Barnes, W. L. Fluorescence near interfaces: the role of photonic mode density. *Journal of Modern Optics* **45**, 661–699 (1998).

[86] Andrew, P. & Barnes, W. L. Energy transfer across a metal film mediated by surface plasmon polaritons. *Science* **306**, 1002–1005 (2004).

[87] Chance, R. R., Prock, A. & Silbey, R. Molecular fluorescence and energy transfer near interfaces. *Advances in Chemical Physics* **37**, 1 (1978).

[88] Drexhage, D. *Progress in Optics XII.* Progress in Optics (North-Holland, Amsterdam, 1974).

[89] Celebi, K. *Organic Electronics (forthcoming).* (2006).

[90] Mamedov, F. & Styring, S. Logistics in the life cycle of photosystem ii - lateral movement in the thylakoid membrane and activation of electron transfer. *Physiologia Plantarum* **119**, 328–336 (2003).